Unconditionally stable small stencil enriched multiple point flux approximations of heterogeneous diffusion problems on general meshes

Julien Coatléven

Submitted preprint

UNCONDITIONALLY STABLE SMALL STENCIL ENRICHED MULTIPLE POINT FLUX APPROXIMATIONS OF HETEROGENEOUS DIFFUSION PROBLEMS ON GENERAL MESHES

Julien Coatléven *†

Abstract. We derive new multiple point flux approximations (MPFA) for the finite volume approximation of heterogeneous and anisotropic diffusion problems on general meshes, in dimension 2 and 3. The resulting methods are unconditionally stable while preserving the small stencil typical of MPFA finite volumes. The key idea is to solve local variational problems with a well designed stabilization term from which we deduce conservative flux instead of directly prescribing a flux formula and solving the usual flux continuity equations. The boundary conditions of our local variational problems are handled through additional cell-centered unknowns, leading to an overall scheme with the same number of unknowns than first-order discontinuous Galerkin methods. Convergence results follow from well established frameworks, while numerical experiments illustrate the good behavior of the method.

Introduction

Diffusion problems occur in many scientific fields such as biology, plasma physics, hydrodynamics, reservoir simulation, etc.. As a consequence, they are probably the most widely studied problems of numerical analysis, and the literature concerning their discretization is tremendous and increasing without end. The most classical approaches to handle diffusion problems are of course the celebrated finite difference, finite element and finite volume methods.

Classical Lagrange finite element methods and their historical variations allow a robust discretization of diffusion on grids with simple cell geometries (mostly simplices and quadrilaterals/hexahedrons, although some finite elements on slightly more general cell types such as pyramids do exist). One of the most ancient extensions of finite elements able to cope with almost any grids are certainly discontinous Galerkin methods (see [13, 29] for a review). More recently mimetic finite differences [16, 15, 25]) or the virtual element method ([23]), even more closely related to classical finite elements, have been proposed as ways to handle complex cell geometries: their success is reflected by the tremendous devoted literature that has appeared in a remarkably short amount of time. They have been extended to most classical problems such as linear ([24, 22]) and non-linear ([26]) elasticity, Stokes' problem ([27]), parabolic problems ([48]), etc.. However successful, those methods are not necessarily the most natural choice for complex flow simulations. Non-linear phenomenons inducing degeneracies are not easy to handle with such formulations, while high-order (or built-in discontinuities in the case of discontinuous Galerkin methods) can induce oscillations or overshoots that cause many troubles when coupling for instance the flow with chemistry.

For those reasons, and also partly for historical reasons, lowest order finite volume methods remain extremely popular in the industry for flow simulations or reservoir engineering. Relatively easy to implement, even in a high performance computing (HPC) context, they allow to solve coupled non linear physical models on the same mesh, while preserving relevant physical properties such as local mass conservation. Undoubtedly and despite its well documented flaws, the most popular finite volume method still remains the two-point flux approximation (TPFA), which leads to compact-stencil, cell-centered, conservative and coercive schemes. Unfortunately, the

*IFP Énergies nouvelles, 1 et 4 avenue de Bois-Préau, 92852 Rueil-Malmaison, France
†julien.coatleven@ifpen.fr

range of mesh satisfying its required orthogonality condition to maintain the method's consistency is relatively small, in particular in presence of anisotropy and strong heterogeneities (see [39]). For this reason, there has always been a strong interest in developing alternative finite volume approaches for general meshes. Quite recently, many finite volume schemes involving additional unknowns have been introduced. Without trying to be exhaustive, let us mention the hybrid finite volume schemes ([40, 41]) and the related mixed finite volumes [34] relying on additional face unknowns, or the vertex based gradient schemes [42, 47] and conservative first order VEM ([20]). We refer the reader to [33] for a relatively recent review. Notice that those methods are closely linked to mimetic finite differences, see [35]. The face based methods have been in some sense generalized through the hybrid high order method (see [32]), which shares many features with virtual element methods. Unsurprisingly, it has also been extended to most classical problems: linear ([31]) and non -linear ([14]) elasticity, fractured porous media flow ([17]), etc.. Despite the many merits of those approaches, one of their main drawback for porous media flow for instance is that their additional unknowns are located on mesh cells boundaries, i.e. on the surfaces of discontinuities of media properties. This leads to some sophisticated handling of those discontinuities (see [44, 43]), considerably complexifying their implementation compared to cell-centered approaches, as well as increasing the stiffness of the linear systems to be solved. Moreover they are not easy to implement in legacy software and even more if a correct handling of discontinuities is required, leading to very intrusive modifications of existing code. Those are probably the main reasons why cell-centered approaches are still favored for instance in many popular industrial porous media flow software.

Consequently, there is still an active literature on cell-centered approximations in general and more specifically on multiple-point flux approximations (MPFA), which are the most natural and maybe oldest extension of the TPFA. The first communications about MPFA methods seem to be [1] and [38]. The key idea is to solve local problems using intermediate unknowns (in general located on mesh cell boundaries) that express flux continuity, and then use those unknowns to derive consistent flux expressions valid for general grids (see [2, 3, 4]). The iconic MPFA method is the so-called MPFA-O method, where the local problems are defined on the set of cells surrounding each vertex, thus forming the "O". Alternative constructions using local domains with different shapes have been developed, the so-called L-, U-, Z- and G- methods (see [7, 45, 6, 9])). Those MPFA methods possess many favorable features: they have a finite volume flux-based formulation, they are cell-centered methods, their stencil is relatively compact, and they are consistent on very general grids. Their only apparent drawback is the fact that the resulting linear system is non-symmetric, preventing the use of some specialized linear solvers. However, as was both observed in practice and later understood theoretically ([8, 5]), they are not unconditionally stable, and do fail on too distorted meshes or in presence of too much anisotropy. Consequently there have also been several alternative attempts to develop unconditionally stable cell-centered schemes, in general using a variational formulation. However, they either lack a clear flux formulation ([19]) or possess a too large stencil making their parallel implementation impractical (see [11, 46]), or both. In fact, looking at those attempts we can infer that using some additional unknowns seems to be quite unavoidable to obtain a stable scheme while maintaining a compact stencil ([19, 11]).

Designing an unconditionally stable, small stencil, cell-centered finite volume method that remains consistent on general meshes is thus still an open problem. In the present paper, we propose new MPFA methods in dimension 2 and 3 that possess all those desired features, at the predictable expense of using additional but cell-centered unknowns. Let us nevertheless mention that our objective here is very practical and consists in offering an alternative to modern finite volume methods that is easier to include in existing cell-centered software. To do so, the key idea to enforce the usual flux continuity is to solve local variational problems using our additional unknowns internal to cells and then deducing the flux formula, instead of prescribing an analytic formula for the flux and then solving the flux continuity equations. Because of those additional unknowns, the resulting schemes have the same number of degrees of freedom than first-order discontinuous Galerkin methods. The idea of using additional cell unknowns for MPFA is not new (see [18]), however they were used as intermediate unknowns to directly enforce flux continuity, and not in the resulting global linear system. Our additional unknowns should thus be compared to the additional face or vertex unknowns of modern finite volume methods ([40, 41, 32, 42, 47]), with the major difference that ours are associated with cells recovering

the "built-in" handling of discontinuities of traditional finite volume methods. In the same way, using local variational problems has also already been tried (see [8]), but without our additional cell unknowns. This combination of approaches will be the key to obtain the desired properties of the resulting MPFA and is, at least to the author's knowledge, completely new as are the resulting schemes.

The paper will be organized as follows: in a first section, we introduce our many notations describing general meshes, describe our model problem and recall what are the main features of MPFA methods using an abstract formulation, emphasizing the underlying mesh partitioning into a submesh. We in particular provide practical examples of mesh partitioning that do not require any complex meshing algorithm and that apply on most meshes encountered in industrial applications. The second section is the heart of the paper: we describe the derivation of our new MPFA methods by solving local variational problems on the subdomains defined by our mesh partitioning. Thanks to the variational formulation of the problem, in the third section we can link our MPFA method with general convergence analysis frameworks, providing convergence results in a rather automatic way. Finally in the fourth section we exhibit numerical results on canonical tests cases of the literature, illustrating the good behavior of the method.

1 Mesh description, model problem and abstract multiple point flux approximations

1.1 Mesh description

From now on, we assume that the domain Ω is a bounded generalized polyhedral (i.e. with potentially non planar faces) included in $\mathbb{R}^d$, $d = 2$ or 3, and $\partial\Omega = \overline{\Omega}\backslash\Omega$ denotes its boundary. A mesh on Ω, denoted by $\mathcal{M}$, is defined as a set $\mathcal{M} = (\mathcal{T}, \mathcal{F}, \mathcal{SF})$ where:

. $\mathcal{T}$ is a finite family of connected open disjoint subsets of Ω (the cells of the mesh), such that $\overline{\Omega} = \cup_{K\in\mathcal{T}}\overline{K}$. For any $K \in \mathcal{T}$, we denote by $|K|$ the d-dimensional Lebesgue measure of K, by h_K the diameter of K, by $\boldsymbol{x}_K$ the barycenter of K.

. $\mathcal{F}$ is a finite family of disjoint subsets of $\overline{\Omega}$ (the faces of the mesh), such that for any $K \in \mathcal{T}$ there exists a subset $\mathcal{F}_K$ of $\mathcal{F}$ such that $\partial K = \cup_{\sigma\in\mathcal{F}_K}\overline{\sigma}$. Then, for any $\sigma \in \mathcal{F}$, we denote by $\mathcal{T}_\sigma = \{K \in \mathcal{T} \mid \sigma \in \mathcal{F}_K\}$ (the neighbours of σ), and assume that either $\mathcal{T}_\sigma$ has exactly one element, and then $\sigma \subset \partial\Omega$ (the set of these faces is denoted $\mathcal{F}_{ext}$), or $\mathcal{T}_\sigma$ has exactly two elements (the set of these faces is denoted $\mathcal{F}_{int}$). For all $K \in \mathcal{T}$ and all $\sigma \in \mathcal{F}_K$, we denote by $\boldsymbol{n}_{K,\sigma}$ the unit normal vector to σ outward to K, by $|\sigma|$ its $d-1$ dimensional Lebesgue measure and by $\boldsymbol{x}_\sigma$ its barycenter.

. $\mathcal{SF}$ is a finite family of disjoint subsets of $\overline{\Omega}$ (the subfaces of the mesh) such that, for all $\zeta \in \mathcal{SF}$, ζ is an open connected subset included in an hyperplane of $\mathbb{R}^d$, whose strictly positive $(d-1)$-dimensional Lebesgue measure is denoted $|\zeta|$. We assume that for any face $\sigma \in \mathcal{F}$, there exists a subset $\mathcal{SF}_\sigma$ of $\mathcal{SF}$ such that $\overline{\sigma} = \bigcup_{\zeta\in\mathcal{SF}_\sigma}\overline{\zeta}$. For any $\zeta \in \mathcal{SF}$, we denote $\boldsymbol{x}_\zeta$ the barycenter of ζ, while for any $K \in \mathcal{T}_\zeta$, we denote $\boldsymbol{n}_{K,\zeta}$ the unit normal vector to ζ outward to K. For any $K \in \mathcal{T}$ we denote $\mathcal{SF}_K = \cup_{\sigma\in\mathcal{F}_K}\mathcal{SF}_\sigma$, and we of course denote $\mathcal{SF}_{ext} = \bigcup_{\sigma\in\mathcal{F}_{ext}}\mathcal{SF}_\sigma$ and $\mathcal{SF}_{int} = \bigcup_{\sigma\in\mathcal{F}_{int}}\mathcal{SF}_\sigma$.

Notice that we do not have assumed that faces are planar in dimension 3: our definition is very permissive and corresponds to the most common practical situations (see figure 1). Further notice that as we in fact already done, some of the above notations describing mesh connectivity will be extended in the natural way in the remaining of the paper without any further mention: for instance, given a subface $\zeta \in \mathcal{SF}$, the set $\mathcal{T}_\zeta$ will denote the cells of whom ζ is a subface, i.e. such that $\zeta \in \mathcal{SF}_\sigma$ for some $\sigma \in \mathcal{F}_K$.

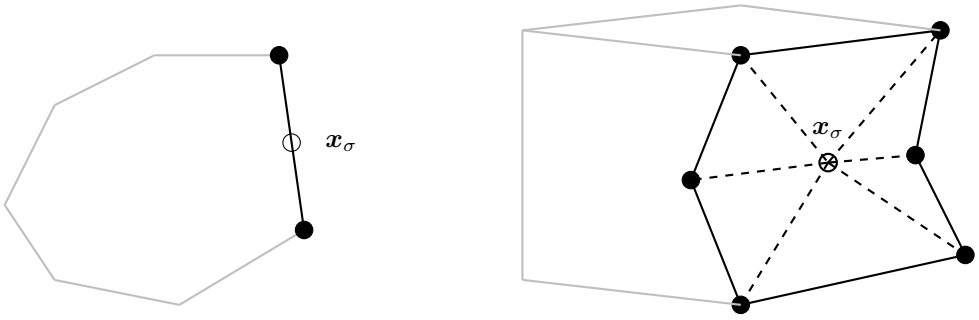

Figure 1: Example of face σ in dimension 2 (left) and 3 (right): full circles are the vertices of σ, the empty circle is $\boldsymbol{x}_\sigma$, dashed lines represent a planar decomposition for face σ in dimension 3

1.2 Model problem

Our model problem will be the most classical diffusion problem:

$$-div\left(\Lambda \nabla \overline{u}\right) = f \quad \text{in } \Omega, \tag{1}$$

complemented with homogeneous Dirichlet boundary conditions:

$$\overline{u} = 0 \text{ on } \partial\Omega, \tag{2}$$

where $\partial\Omega = \overline{\Omega}\backslash\Omega$ is the boundary of the domain Ω, under the additional hypothesis that $f \in L^2(\Omega)$ and that Λ is a measurable function from Ω to $\mathbb{M}_d(\mathbb{R})$, the set of $d \times d$ matrices, and such that for almost every (a.e.) $\boldsymbol{x} \in \Omega$, $\Lambda(\boldsymbol{x})$ is symmetric, positive definite and there exists two strictly positive real numbers λ_*, λ^* such that for every $\boldsymbol{\xi} \in \mathbb{R}^d$:

$$\lambda_* |\boldsymbol{\xi}|^2 \leqslant \Lambda(\boldsymbol{x})\boldsymbol{\xi} \cdot \boldsymbol{\xi} \leqslant \lambda^* |\boldsymbol{\xi}|^2. \tag{3}$$

1.3 Abstract multiple point flux approximation

1.3.1 General formulation

We are now going to give a very general definition of multiple point flux approximations, in order to be able to precisely describe what are the desired consistency and stability properties. If the notations and definitions introduced here will serve as a guideline to describe our unconditionally stable MPFA, notice that apart from the additional cell unknowns most of this subsection is completely classical, and of course no true originality is claimed here. Our enriched set of degrees of freedom for cell-centered methods is given by

$$X_{\mathcal{T}} = \left\{ ((v_K)_{K\in\mathcal{T}}, (\boldsymbol{V}_K)_{K\in\mathcal{T}}, (v_\sigma)_{\sigma\in\mathcal{F}_{ext}}) \mid v_K \in \mathbb{R}, \boldsymbol{V}_K \in \mathbb{R}^d \ \ \forall K \in \mathcal{T} \text{ and } v_\sigma \in \mathbb{R} \ \ \forall \sigma \in \mathcal{F}_{ext} \right\}, \tag{4}$$

where we denote by convention with a bold capital letter any element $\boldsymbol{V}_{\mathcal{T}}$ of $X_{\mathcal{T}}$. The boundary face values $\boldsymbol{V}_{\mathcal{T}}^{ext} = (v_\sigma)_{\sigma\in\mathcal{F}_{ext}}$ are introduced to handle boundary conditions, which is classically done with a single unknown per face in many commercial simulators. In the case of homogeneous Dirichlet boundary conditions, this naturally leads to defining the space

$$X_{\mathcal{T},0} = \left\{ \boldsymbol{V}_{\mathcal{T}} \in X_{\mathcal{T}} \mid \boldsymbol{V}_{\mathcal{T}}^{ext} = 0 \right\}. \tag{5}$$

For each cell $K \in \mathcal{T}$, the unknowns $\boldsymbol{V}_K \in \mathbb{R}^d$ associated with each cell are our additional unknowns compared to classical MPFA methods, hence the name "enriched" for our new MPFA methods.

In general, multiple point flux approximation will also involve a set of intermediate degrees of freedom X^{in} whose elements denoted $\boldsymbol{V}^{in}$ do not appear in the final formulation. In practice the intermediate unknowns $\boldsymbol{U}^{in}$ are always computed by solving intermediate problems, allowing to express the components of $\boldsymbol{U}^{in}$ as functions of the components of $\boldsymbol{U}_{\mathcal{T}}$, in general using only those elements of $\boldsymbol{U}_{\mathcal{T}}$ that are geometrically located immediately around the considered component of $\boldsymbol{U}^{in}$. For instance, in dimension 2 for the MPFA-O scheme each intermediate unknown is associated to a subface ζ surrounding an internal vertex s, and is expressed as a function of the cell unknowns surrounding the vertex. We sum up all the possible choices by assuming that we are given an operator $\boldsymbol{I}^{in} : X_{\mathcal{T}} \longmapsto X^{in}$ such that the solution to the MPFA approximation has to satisfy the relation:

$$\boldsymbol{U}^{in} = \boldsymbol{I}^{in}(\boldsymbol{U}_{\mathcal{T}}). \tag{6}$$

Along with the precise expression of the flux, the choice of operator $\boldsymbol{I}^{in}$ fully defines the MPFA method. To simplify many expressions in the following, we will transfer the boundary conditions to the subfaces using the set X^{ext} of intermediate unknowns associated to exterior subfaces

$$X^{ext} = \left\{ \boldsymbol{V}^{ext} = (v_\zeta)_{\zeta \in \mathcal{SF}_{ext}} \mid v_\zeta \in \mathbb{R} \ \ \forall\, \zeta \in \mathcal{SF}_{ext} \right\}, \tag{7}$$

and a transfer operator $\boldsymbol{I}^{ext} : X_{\mathcal{T}} \longmapsto X^{ext}$ defined by setting:

$$\boldsymbol{U}^{in,ext} = \boldsymbol{I}^{ext}(\boldsymbol{U}^{ext}_{\mathcal{T}}) \quad \Longleftrightarrow \quad u_\zeta = I_\zeta(\boldsymbol{U}^{ext}_{\mathcal{T}}) = u_\sigma \ \ \forall\, \sigma \in \mathcal{F}_{ext},\ \forall\, \zeta \in \mathcal{SF}_\sigma, \tag{8}$$

and assuming that we always have $X^{ext} \subset X^{in}$. As for inhomogeneous boundary conditions, this would lead to an approximation of order h, this choice might seem peculiar, however we do so to fully match what is a common practice: in legacy software the boundary conditions data is not given on subfaces, but on full faces. Using those notations, the MPFA methods we are interested in take the general form

$$\left| \begin{array}{ll} \displaystyle\sum_{\zeta \in \mathcal{SF}_K} F_{K,\zeta}(\boldsymbol{U}_{\mathcal{T}}, \boldsymbol{U}^{in}) = |K| f_K & \forall\, K \in \mathcal{T}, \\ u_\sigma = 0 & \forall\, \sigma \in \mathcal{F}_{ext}, \\ \boldsymbol{U}_K = \boldsymbol{G}_K(\boldsymbol{U}_{\mathcal{T}}) & \forall\, K \in \mathcal{T}, \\ \boldsymbol{U}^{in} = \boldsymbol{I}^{in}(\boldsymbol{U}_{\mathcal{T}}), & \end{array} \right. \tag{9}$$

where for all $K \in \mathcal{T}$ f_K is in general chosen to be equal to $f_K = \frac{1}{|K|}\int_K f$ and the "gradient" operator $\boldsymbol{G}$ is in principle an approximation of the solution gradient $\boldsymbol{G}_K(\boldsymbol{U}_{\mathcal{T}}) \approx \nabla \overline{u}|_K$. The flux functions are constructed in such a way that they satisfy the following conservation properties:

$$\sum_{K \in \mathcal{T}_\zeta} F_{K,\zeta}(\boldsymbol{U}_{\mathcal{T}}, \boldsymbol{U}^{in}) = 0 \quad \forall\, \zeta \in \mathcal{SF}_{in}, \tag{10}$$

and are in principle an approximation of the solution's flux:

$$F_{K,\zeta}(\boldsymbol{U}_{\mathcal{T}}, \boldsymbol{U}^{in}) \approx -\int_\zeta \Lambda|_K \nabla \overline{u} \cdot \boldsymbol{n}_{K,\zeta}.$$

Notice that with a slight abuse of notations the effective flux can be defined as depending only on the desired "cell-centered" unknowns $\boldsymbol{U}_{\mathcal{T}}$, as we can write:

$$F_{K,\zeta}(\boldsymbol{U}_{\mathcal{T}}) = F_{K,\zeta}(\boldsymbol{U}_{\mathcal{T}}, \boldsymbol{I}^{in}(\boldsymbol{U}_{\mathcal{T}})). \tag{11}$$

This is the usual form under which the flux is used in practice, using only the "cell-centered" unknowns. Completely defining a MPFA method can thus be sum up as choosing operators $\boldsymbol{I}^{in}$ and $\boldsymbol{G}_{\mathcal{T}} = (\boldsymbol{G}_K)_{K \in \mathcal{T}}$, as well as an expression for the flux $(F_{K,\zeta})_{K \in \mathcal{T}, \zeta \in \mathcal{SF}_K}$.

Remark 1.1. The mappings $\boldsymbol{I}^{ext}$ that we have used to describe boundary conditions are obviously not the only possible choice for inhomogeneous Dirichlet boundary conditions. The most natural alternative, if one enjoys a sufficiently precise description of boundary conditions through some function $g \in C^0(\partial\Omega)$ is to use $I_\zeta = g(\boldsymbol{x}_\zeta)$, or classical integral alternatives for $g \in H^{1/2}(\partial\Omega)$. Another alternative that would be more practical for existing software would be to construct the I_ζ as barycentric interpolators from the available boundary data and thus from the $(u_\sigma)_{\sigma\in\mathcal{F}}$. Notice that this might increase the stencil of boundary cells with boundary faces from surrounding cells.

1.3.2 Submeshes and intermediate unknowns

To fix ideas on the set of intermediate unknowns X^{in} and as it will correspond to our needs, we introduce a submesh based on the subfaces of the original mesh and on an additional set $\mathcal{IF}$ of internal faces, defined as follows:

. $\mathcal{IF}$ is a finite family of disjoint subsets of $\overline{\Omega}$ such that, for all $\zeta \in \mathcal{SF}$, ζ is an open connected subset included in a hyperplane of $\mathbb{R}^d$, whose strictly positive $(d-1)$-dimensional Lebesgue measure is denoted $|\zeta|$. We assume that for any $\zeta \in \mathcal{IF}$, there exists exactly one $K \in \mathcal{T}$ such that $\overset{\circ}{\zeta} \subset \overset{\circ}{K}$, and we denote $\mathcal{T}_\zeta = \{K\}$. For any $\zeta \in \mathcal{IF}$, we denote $\boldsymbol{x}_\zeta$ the barycenter of ζ, while for any $K \in \mathcal{T}$, we denote $\mathcal{IF}_K = \{\zeta \in \mathcal{IF} \mid K \in \mathcal{T}_\zeta\}$.

Then, $\mathcal{SM} = (\mathcal{ST}, \{\mathcal{SF}, \mathcal{IF}\}, \{\mathcal{SF}, \mathcal{IF}\})$ is a mesh in the sense of section 1.1, whose faces are all planar and such that the set of faces and subfaces are identical. Notice that by construction, we have:

$$\mathcal{IF} = \bigcup_{K\in\mathcal{T}} \mathcal{IF}_K.$$

We assume that there exists a partition of $\mathcal{ST}$ into $N_\mathcal{P}$ subsets, indexed by the elements p of a partitioning set $\mathcal{P}$ of size $N_\mathcal{P}$, and such that for any $K \in \mathcal{T}$ there exists a subset $\mathcal{P}_K$ of $\mathcal{P}$ defining a partitioning of cell K:

$$\overline{K} = \bigcup_{p\in\mathcal{P}_K} \overline{K_p} \quad \text{for all } K \in \mathcal{T},$$

where $K_p \in \mathcal{ST}$ for all $p \in \mathcal{P}_K$, and that

$$\mathcal{ST} = \bigcup_{p\in\mathcal{P}} \mathcal{ST}_p \quad \text{where} \quad \mathcal{ST}_p = \{K_p \in \mathcal{ST} \mid K \in \mathcal{T}_p\} \quad \text{and} \quad \mathcal{T}_p = \{K \in \mathcal{T} \mid p \in \mathcal{P}_K\}.$$

The exact choice of the subcells K_p will define the local domains $D_p = \bigcup_{K\in\mathcal{T}_p} K_p$ on which the MPFA intermediate problems will be solved. They however have to fulfill a few requirements: denoting for any $K \in \mathcal{T}$ and any $p \in \mathcal{P}_K$

$$\mathcal{F}_{K,p} = \mathcal{IF}_{K,p} \cup \mathcal{SF}_{K,p} \quad \text{and} \quad \mathcal{SF}_{K,p} = \{\zeta \in \mathcal{SF}_K \mid \zeta \subset \partial K_p\} \quad \text{and} \quad \mathcal{IF}_{K,p} = \{\zeta \in \mathcal{IF}_K \mid \zeta \subset \partial K_p\},$$

we assume that for any $K \in \mathcal{T}$ and $p \in \mathcal{P}$, we have

$$\overline{\partial K_p \cap \partial K} = \bigcup_{\zeta\in\mathcal{SF}_{K,p}} \overline{\zeta} \subset \bigcup_{\zeta\in\mathcal{SF}_K} \overline{\zeta} \quad \text{and} \quad \overline{\partial K_p}\backslash(\partial K_p \cap \partial K) = \bigcup_{\zeta\in\mathcal{IF}_{K,p}} \overline{\zeta} \subset \bigcup_{\zeta\in\mathcal{IF}_K} \overline{\zeta},$$

as well as

$$\partial D_p \subset \left(\bigcup_{\zeta\in\mathcal{IF}_K, K\in\mathcal{T}_p} \overline{\zeta} \right) \cup \left(\bigcup_{\zeta\in\mathcal{SF}_K\cap\mathcal{SF}_{ext}, K\in\mathcal{T}_p} \right) \quad \text{where} \quad D_p = \bigcup_{K\in\mathcal{T}_p} K_p.$$

Notice that as a consequence of the definition of cells and faces in section 1.1, for any $K \in \mathcal{T}$ all the K_p with $p \in \mathcal{P}_K$ being disjoint we get that for any $K \in \mathcal{T}$ and any $\zeta \in \mathcal{SF}_K$ there exists a unique $p \in \mathcal{P}_K$ such that $\zeta \subset \partial K_p$. Finally for any $p \in \mathcal{P}$ we of course denote:

$$\mathcal{F}_p = \bigcup_{K\in\mathcal{T}_p} \mathcal{F}_{K,p} \quad \text{and} \quad \mathcal{SF}_p = \bigcup_{K\in\mathcal{T}_p} \mathcal{SF}_{K,p} \quad \text{and} \quad \mathcal{IF}_p = \bigcup_{K\in\mathcal{T}_p} \mathcal{IF}_{K,p}.$$

Finally, notice that as a consequence of the above definitions for any $\zeta \in \mathcal{IF}_K$ there exists exactly two elements p_1 and p_2 in $\mathcal{P}$ such that $\zeta \in \mathcal{IF}_{K,p_1} \cap \mathcal{IF}_{K,p_2}$, and we denote $\mathcal{P}_\zeta = \{p_1, p_2\}$.

In other words, those abstract requirements simply mean that all the cells $K \in \mathcal{T}$ of the original mesh are divided into subcells with one subcell K_p for each $p \in \mathcal{P}_K$, the boundary of K_p being composed of elements of $\mathcal{SF}_K$ (i.e. subfaces of cell K) for its part included in ∂K, the remaining part being composed of elements of $\mathcal{IF}_K$ (i.e. subfaces internal to cell K). We give examples in the next subsection to both make things clearer and provide practical ways of obtaining a good submesh in many situations that do not even require resorting to a mesh generator.

Our new MPFA methods will use the following set of intermediate internal unknowns:

$$X^{in} = \left\{ \boldsymbol{V}^{in} = \left((v_{K,p,\zeta'})_{K\in\mathcal{T}, p\in\mathcal{P}_K, \zeta'\in\mathcal{IF}_{K,p}}, (v_\zeta)_{\zeta\in\mathcal{SF}} \right) \mid v_{K,p,\zeta'} \in \mathbb{R} \ \ \forall K \in \mathcal{T}, \ \ \forall\, p \in \mathcal{P}_K, \ \ \forall\, \zeta^{'} \in \mathcal{IF}_{K,p} \right.$$
$$\left. \text{and } v_\zeta \in \mathbb{R} \ \ \forall\, \zeta \in \mathcal{SF} \right\}, \tag{12}$$

where in each cell K the unknowns $v_{K,p,\zeta'}$ are unknowns associated to the barycenters $\boldsymbol{x}_{\zeta'}$ of the internal subfaces of cell K. As the notation suggests, we associate to each internal subface $\zeta^{'} \in \mathcal{IF}_K$ two values, one for each side of $\zeta^{'}$, allowing jumps inside the cell K but not on its boundary. This should be compared to discontinuous Galerkin methods, for which jumps are allowed on the boundary of the cell but not inside.

1.4 Examples of partitioning for meshes with star-shaped cells

Given a mesh $\mathcal{M} = (\mathcal{T}, \mathcal{F}, \mathcal{SF})$, let us denote $\mathcal{V}$ the set of vertices of the mesh and $\mathcal{E}$ the set of edges of the mesh . For all $s \in \mathcal{V}$, we denote $\mathcal{SF}_s$ the set $\{\zeta \in \mathcal{SF} \mid s \in \zeta\}$, and $\mathcal{T}_s$ the set of cells $\{K \in \mathcal{T} \mid s \in \overline{K}\}$. For all $K \in \mathcal{T}$, the set $\mathcal{V}_K$ stands for $\{s \in \mathcal{V} \mid K \in \mathcal{T}_s\}$, while for all $\zeta \in \mathcal{SF}$, the set $\mathcal{V}_\zeta$ stands for $\{s \in \mathcal{V} \mid \zeta \in \mathcal{SF}_s\}$. For all $e \in \mathcal{E}$ there exists a set $\mathcal{V}_e$ of exactly two vertices such that $\overline{e} = Conv((\boldsymbol{x}_s)_{s\mathcal{V}_e})$ (where $Conv$ denotes the convex hull of a set of points). In dimension 2, we have $\mathcal{F} = \mathcal{E}$ while in dimension 3, for any $\zeta \in \mathcal{SF}$, there exists a subset $\mathcal{E}_\zeta$ of $\mathcal{E}$ such that $\partial\zeta = \cup_{e\in\mathcal{E}_\zeta} \overline{e}$ and we have $\mathcal{E} = \cup_{\zeta\in\mathcal{SF}} \mathcal{E}_\zeta$. For any $s \in \mathcal{V}$, the geometrical position of the vertex will be denoted $\boldsymbol{x}_s$ while for any $e \in \mathcal{E}$, we denote by $\boldsymbol{x}_e$ its barycenter..

In this subsection, we assume that for any $K \in \mathcal{T}$, K is star-shaped with respect to $\boldsymbol{x}_K$.

1.4.1 Face and subface based partitioning

In the case of a mesh with star-shaped cells, the simplest and probably most natural choices of partitioning sets consist in using either the faces $\mathcal{P} = \mathcal{F}$ or the subfaces $\mathcal{P} = \mathcal{SF}$. For those two cases, we respectively define for any $K \in \mathcal{T}$:

$$K_\sigma = Conv(\boldsymbol{x}_K, \sigma) \quad \text{for any } \sigma \in \mathcal{F}_K \quad \text{and} \quad K_\zeta = Conv(\boldsymbol{x}_K, \zeta) \quad \text{for any } \zeta \in \mathcal{SF}_K.$$

In other words, in dimension 2 K_σ (respectively K_ζ) is the simplex formed by $\boldsymbol{x}_K$ and the vertices of σ (respectively of ζ), i.e. $K_\sigma = Conv(\boldsymbol{x}_K, (\boldsymbol{x}_s)_{s\in\mathcal{V}_\sigma})$ (respectively $K_\zeta = Conv(\boldsymbol{x}_K, (\boldsymbol{x}_s)_{s\in\mathcal{V}_\zeta})$). In dimension 3 their structure is more involved, and K_σ (respectively K_ζ) is the generalized polyhedron delimited by σ and the triangles formed by $\boldsymbol{x}_K$ and the edges of σ (respectively ζ). More precisely, we have in the case of faces $\mathcal{P} = \mathcal{F}$ and $\mathcal{P}_K = \mathcal{F}_K$ for all $K \in \mathcal{T}$:

$$\partial K_\sigma = \overline{\sigma} \cup \bigcup_{\zeta'\in\mathcal{IF}_{K,\sigma}} \overline{\zeta}^{'}$$

where

$$\mathcal{IF}_{K,\sigma} = \bigcup_{s\in\mathcal{V}_\sigma} Conv(\boldsymbol{x}_K, \boldsymbol{x}_s) \quad \text{if } d = 2 \quad \text{and} \quad \mathcal{IF}_{K,\sigma} = \bigcup_{e\in\mathcal{E}_\sigma} Conv(\boldsymbol{x}_K, (\boldsymbol{x}_s)_{s\in\mathcal{V}_e}) \quad \text{if } d = 3,$$

and similarly in the case of subfaces $\mathcal{P} = \mathcal{SF}$and $\mathcal{P}_K = \mathcal{SF}_K$ for all $K \in \mathcal{T}$:

$$\partial K_\zeta = \overline{\zeta} \cup \bigcup_{\zeta' \in \mathcal{IF}_{K,\zeta}} \overline{\zeta}',$$

where

$$\mathcal{IF}_{K,\zeta} = \bigcup_{s \in \mathcal{V}_\zeta} Conv(\boldsymbol{x}_K, \boldsymbol{x}_s) \quad \text{if } d = 2 \quad \text{and} \quad \mathcal{IF}_{K,\zeta} = \bigcup_{e \in \mathcal{E}_\zeta} Conv(\boldsymbol{x}_K, (\boldsymbol{x}_s)_{s \in \mathcal{V}_e}) \quad \text{if } d = 3.$$

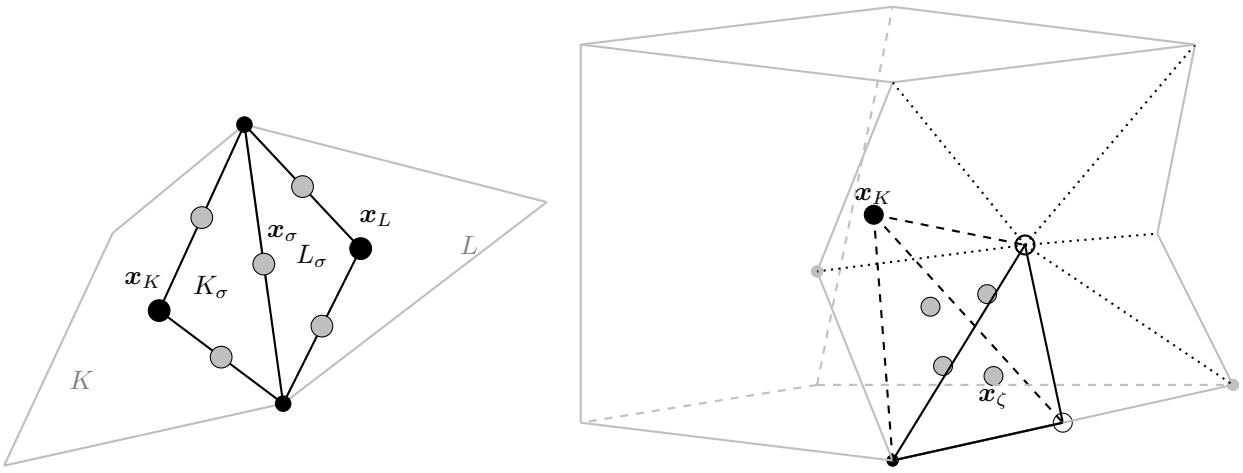

Figure 2: Example of domain D_σ in dimension 2 (left) and half domain D_ζ in dimension 3 (right): empty circles are face centers, grey circles are the location of the unknowns of the local variational problem

1.4.2 O-shape partitioning

Assume that for any $\sigma \in \mathcal{F}$, σ is star-shaped with respect to $\boldsymbol{x}_\sigma$, and (see figure 3) that for any subface $\zeta \in \mathcal{SF}_\sigma$ in dimension 2 there exists a vertex $s \in \mathcal{V}_\sigma$ such that $\overline{\zeta} = \overline{\zeta}(\sigma, s) = Conv(\boldsymbol{x}_\sigma, \boldsymbol{x}_s)$ while in dimension 3 (see figure 3) there exists an edge $e \in \mathcal{E}_\sigma$ and a vertex $s \in \mathcal{V}_\sigma \cap \mathcal{V}_e$ such that $\overline{\zeta} = \overline{\zeta}(\sigma, e, s) = Conv(\boldsymbol{x}_\sigma, \boldsymbol{x}_e, \boldsymbol{x}_s)$. For future reference, we say that such a mesh has simplicial half-edge based subfaces. Half-edge based subfaces can be defined for meshes resulting from deformations obtained by moving vertices of polytops which are very common in industrial applications. Then, for any $K \in \mathcal{T}$ and any $\zeta \in \mathcal{SF}_K$, the set K_ζ is naturally defined as $\overline{K}_\zeta = Conv(\boldsymbol{x}_K, (\boldsymbol{x}_s)_{s \in \mathcal{V}_\zeta})$, i.e. the simplex formed by the vertices of ζ and $\boldsymbol{x}_K$, such that we get:

$$\overline{K} = \bigcup_{\zeta \in \mathcal{SF}_K} \overline{K}_\zeta.$$

The O-shaped partitioning, clearly corresponding to the classical MPFA-O method, consists in choosing $\mathcal{P} = \mathcal{V}$ with $\mathcal{P}_K = \mathcal{V}_K$ for all $K \in \mathcal{T}$ on a mesh with simplicial half-edge based subfaces. For any vertex $s \in \mathcal{V}$, and any $K \in \mathcal{T}_s$, we set:

$$\overline{K_s} = \bigcup_{\zeta \in \mathcal{SF}_K \cap \mathcal{SF}_s} \overline{K}_\zeta \quad \text{with} \quad \partial K_s = \bigcup_{\zeta \in \mathcal{SF}_s} \overline{\zeta} \cup \bigcup_{\zeta' \in \mathcal{IF}_{K,s}} \overline{\zeta}'.$$

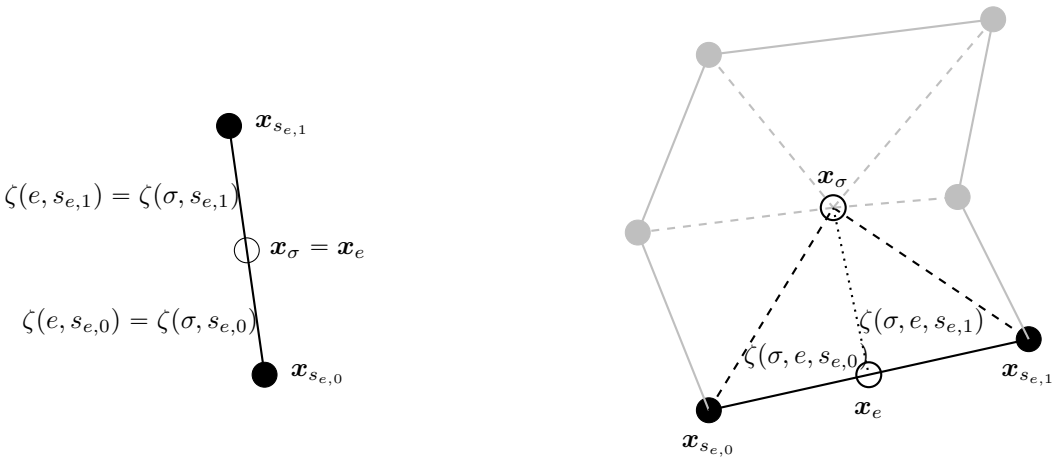

Figure 3: Example of face decomposition in dimension 2 (left) and 3 (right)

Recalling that D_s is given by:

$$\overline{D_s} = \bigcup_{K \in \mathcal{T}_s} \overline{K}_s, \tag{13}$$

we see on figure 4 that the internal faces of D_s are precisely the subfaces $\zeta \in \mathcal{SF}_s$, that is to say the subfaces on which we want to construct our half flux. We also recognize on figure 4 the "O" shape of domain D_s in dimension 2 (its generalization to dimension 3 while easy to construct in practice is unfortunately quite hard to draw).

Remark 1.2. The partitioning $\mathcal{P}$ and associated subcells K_p can be fairly more general than the examples presented above in the case of meshes with a star-shaped cells. First, even in the case of meshes with simplicial half-edge based subfaces it is clear that we could replace the O domains by domains looking like any of the classical MPFA domains (i.e. the L, U, G or Z domains). It is also clear that there are ways to combine those domains and still fulfill the partitioning requirements. For very complex cells however, one will have to use a mesh generator to obtain the submesh and thus the partitioning. We do believe that most industrial software use simple enough cells to allow using one or a combination of the approaches that we have detailed.

2 Derivation of stable multi-point flux approximations

The principle of most classical MPFA methods and in particular the MPFA-O method (see [2, 3, 4, 1]) is to solve on the local domain D_p a local problem involving functions w that are affine in each $K_p \in \mathcal{T}_p$ (i.e. $w|_{K_p} \in \mathbb{P}_1(K_p)$), such that $w(\boldsymbol{x}_K) = u_K$ for $K \in \mathcal{T}_p$, and such that the trace of $\Lambda \nabla w$ is continuous across the subfaces $\mathcal{SF}_p$ included in D, i.e.:

$$\sum_{K \in \mathcal{T}_p \cap \mathcal{T}_\zeta} \Lambda_K \nabla w \cdot \boldsymbol{n}_{K,\zeta} = 0 \quad \forall\, \zeta \in \mathcal{SF}_p, \tag{14}$$

along with some extra continuity conditions inside D_p or on its boundary to close the system (in particular in the case of the L-method, see [7]). Then, the flux $F_{K,\zeta}$ are simply defined as $-|\zeta| \Lambda_K \nabla w \cdot \boldsymbol{n}_{K,\zeta}$. Here, we will follow a closely related but nevertheless different approach. On each domain D_p we will solve a local variational problem whose governing idea is the following: if w is defined on D_p and satisfies the requirements of the MPFA-O method, then as Λ is assumed constant on each $K \in \mathcal{T}$ we get

$$-div(\Lambda_K \nabla w) = 0 \quad \text{ in } K_p \text{ for all } K \in \mathcal{T}_p, \tag{15}$$

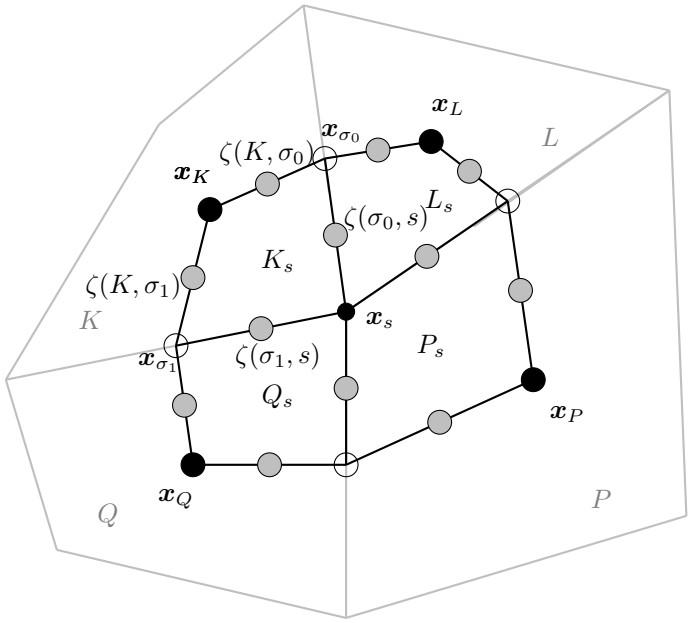

Figure 4: Example of domain around an internal vertex in dimension 2 for the O-shaped partitioning: empty circles are face centers, grey circles are the location of the intermediate unknowns of the local problem

as its gradient is constant in each $K \in \mathcal{T}_s$ which combined with (14) implies that $div(\Lambda_K \nabla w) = 0$ in all D_p. To derive our multiple-point flux, we will solve a local variational problem that is roughly speaking a discrete counterpart of (15) on D_p. The solution to this local problem will define the mappings I_ζ, while the flux $F_{K,\zeta}$ will simply be taken as equal to the flux of the local variational problems.

Consequently, the starting point of this section will consists in describing the local variational problems on each D_p. Then, after providing details on the obtained flux formula, we will explain how to construct the mappings $\boldsymbol{G}_K$ in a way ensuring the stability of the method. To do so, we will choose the $\boldsymbol{G}_K$'s such that we can reinterpret the local variational problems as parts of a global discrete variational formulation. After providing some implementations details, we conclude this section by establishing stability using the global variational formulation. The principles of the enriched MPFA method are in fact independent of the choice of partitioning set $\mathcal{P}$. The main difficulty is in fact due to notations: we have tried (and probably failed) to reduce notational cumbersomeness by using abstract notations for the intermediate unknowns internal to cells, allowing us to deal with dimension 2 and 3 at the same time, for any choice of partitioning set $\mathcal{P}$.

2.1 The local variational problem on D_p

For any $p \in \mathcal{P}$, the set of degrees of freedom involved in the local variational problem on D_p is given by:

$$X_p = \left\{ \boldsymbol{V}_p = \left((v_K, \boldsymbol{V}_K))_{K \in \mathcal{T}_p}, (v_\sigma)_{\sigma \in \mathcal{F}_p \cap \mathcal{F}_{ext}}, (v_\zeta)_{\zeta \in \mathcal{SF}_p}, (v_{K,p,\zeta'})_{\zeta' \in \mathcal{IF}_p} \right) \right\}. \tag{16}$$

As we consider a fixed $p \in \mathcal{P}$ in all this subsection and as an internal subface belongs to only one cell K, to simplify the notation we momentarily denote $v_{\zeta'}$ instead of $v_{K,p,\zeta'}$, and thus

$$X_p = \left\{ \boldsymbol{V}_p = \left((v_K, \boldsymbol{V}_K))_{K \in \mathcal{T}_p}, (v_\sigma)_{\sigma \in \mathcal{F}_p \cap \mathcal{F}_{ext}}, (v_{\zeta'})_{\zeta' \in \mathcal{F}_p} \right) \right\}, \tag{17}$$

but it is important to keep in mind that they correspond to different values from one subcell to another, in particular when going back to the global problem. Any element $\boldsymbol{V}_p$ of X_p is subdivided into two sets of degrees of freedom $\boldsymbol{V}_p = (\boldsymbol{V}_{\mathcal{T}_p}, \boldsymbol{V}_p^{in})$, where

$$\boldsymbol{V}_{\mathcal{T}_p} = ((v_K, \boldsymbol{V}_K)_{K\in\mathcal{T}_p}, (v_\sigma)_{\sigma\in\mathcal{F}_p\cap\mathcal{F}_{ext}}) = ((v_K, \boldsymbol{V}_K)_{K\in\mathcal{T}_p}, \boldsymbol{V}_{\mathcal{T}_p}^{ext}),$$

are the local "cell-centered" unknowns and

$$\boldsymbol{V}_p^{in} = \left(v_{\zeta'}\right)_{\zeta'\in\mathcal{F}_p} = \left(\boldsymbol{V}_p^{ext}, (v_\zeta)_{\zeta\in\mathcal{SF}_p\cap\mathcal{SF}_{int}}, (v_{\zeta'})_{\zeta'\in\mathcal{IF}_p}\right),$$

the intermediate unknowns. For any $\zeta \in \mathcal{SF}_{ext}$ as the operator I_ζ was initially defined as operating on the full set of unknowns $\boldsymbol{V}_\mathcal{T}$, with a slight abuse of notations we denote

$$\boldsymbol{I}_p^{ext}(\boldsymbol{V}_{\mathcal{T}_p}^{ext}) = (I_\zeta^{ext}(\boldsymbol{V}_{\mathcal{T}_p}^{ext}))_{\zeta\in\mathcal{SF}_p\cap\mathcal{SF}_{ext}} \quad \text{with} \quad I_\zeta^{ext}(\boldsymbol{V}_{\mathcal{T}_p}^{ext}) = v_\sigma \quad \text{if } \zeta \in \mathcal{SF}_\sigma \cap \mathcal{SF}_p \quad \text{and} \quad \sigma \in \mathcal{F}_{ext}.$$

Given $\boldsymbol{U}_{\mathcal{T}_p}$, we denote

$$X_p(\boldsymbol{U}_{\mathcal{T}_p}) = \left\{\boldsymbol{V}_p \in X_p \mid \boldsymbol{V}_{\mathcal{T}_p} = \boldsymbol{U}_{\mathcal{T}_p} \text{ and } \boldsymbol{V}_p^{ext} = \boldsymbol{I}_p^{ext}(\boldsymbol{V}_{\mathcal{T}_p}^{ext})\right\}. \tag{18}$$

Finally let us introduce the hybrid reconstruction (see [40, 41]) operator $\Pi_{K,p} : X_p \longmapsto \mathbb{P}_1(\mathbb{R})$ on K_p:

$$\Pi_{K,p}(\boldsymbol{W}_p)(\boldsymbol{x}) = w_K + \nabla\Pi_{K,p}(\boldsymbol{W}_p)\cdot(\boldsymbol{x} - \boldsymbol{x}_K) \quad \text{with} \quad \nabla\Pi_{K,p}(\boldsymbol{W}_p) = \sum_{\zeta\in\mathcal{F}_{K,p}} \frac{|\zeta|}{|K_p|}(w_\zeta - w_K)\boldsymbol{n}_{K,p,\zeta},$$

with $\boldsymbol{n}_{K,p,\zeta}$ the outgoing normal for K_p along its planar boundary part $\zeta^{'}$. We denote:

$$\theta_\Pi = \sup_{K\in\mathcal{T}}\sup_{p\in\mathcal{P}_K}\sup_{\zeta\in\mathcal{F}_{K,p}} \max\left(h_{K_p}|\zeta|\,|K_p|^{-1}, h_{K_p}^{-1}|\zeta|^{-1}\,|K_p|\right),$$

and

$$\theta_\mathcal{F} = \sup_{K\in\mathcal{T}}\sup_{p\in\mathcal{P}_K} card(\mathcal{F}_{K,p}) \quad \text{and} \quad \theta_\mathcal{P} = \sup_{K\in\mathcal{T}} card(\mathcal{P}_K),$$

the quality parameters of the subcells, where h_{K_p} is of course the diameter of the subcell K_p. Still following the ideas of the MPFA-O method but in a variational fashion, we will consider the following discrete counterpart of (15) on D_p with Neumann boundary conditions:

$$\left|\begin{array}{ll} -div(\Lambda_K\nabla w) = 0 & \text{in all } K_p \in D_p, \\ -\Lambda_K\nabla w\cdot\boldsymbol{n}_{D_p} = -\Lambda_K\boldsymbol{U}_K\cdot\boldsymbol{n}_{D_p} & \text{on } \partial D_p\backslash(\partial D_p\cap\partial\Omega), \\ w = u_\sigma & \text{on all } \sigma\subset\partial D_p\cap\partial\Omega. \end{array}\right.$$

Consequently, our local variational problem consists in finding $\boldsymbol{W}_p \in X_p(\boldsymbol{U}_{\mathcal{T}_p})$ such that

$$0 = a_p(\boldsymbol{W}_p, \boldsymbol{V}_p) = a_p^0(\boldsymbol{W}_p, \boldsymbol{V}_p) - \sum_{K\in\mathcal{T}_p}\sum_{\zeta\in\mathcal{IF}_{K,p}} |\zeta|\Lambda_K\boldsymbol{W}_K\cdot\boldsymbol{n}_{K,p,\zeta}v_\zeta \quad \forall\, \boldsymbol{V}_p \in X_p(0), \tag{19}$$

where

$$a_p^0(\boldsymbol{W}_p, \boldsymbol{V}_p) = \sum_{K\in\mathcal{T}_p} |K_p|\Lambda_K\nabla\Pi_{K,p}(\boldsymbol{W}_p)\cdot\nabla\Pi_{K,p}(\boldsymbol{V}_p) + s_{K,p}(\boldsymbol{W}_p, \boldsymbol{V}_p), \tag{20}$$

and where the stabilization bilinear form is given by

$$s_{K,p}(\boldsymbol{W}_p, \boldsymbol{V}_p) = \sum_{\zeta\in\mathcal{F}_{K,p}} \lambda_{K,p,\zeta}^0\left(w_\zeta - \Pi_{K,p}(\boldsymbol{W}_p)(\boldsymbol{x}_\zeta)\right)\left(v_\zeta - \Pi_{K,p}(\boldsymbol{V}_p)(\boldsymbol{x}_\zeta)\right)$$

$$+\lambda^1_{K,p}(\boldsymbol{W}_K - \nabla\Pi_{K,p}(\boldsymbol{W}_p)) \cdot (\boldsymbol{V}_K - \nabla\Pi_{K,p}(\boldsymbol{V}_p)), \tag{21}$$

where denoting for some $0 \leqslant \omega \leqslant 1$, $0 < \gamma_0 < 1$ and $\gamma_1 > 0$:

$$\lambda_{K,p,\zeta} = (1-\omega)\Lambda_K \boldsymbol{n}_{K,p,\zeta} \cdot \boldsymbol{n}_{K,p,\zeta} + \omega||\Lambda_K||_2 \quad \text{and} \quad \gamma_{K,p,\mu} = \frac{\gamma_0|K_p|}{(1+\mu)\left(\sum_{\zeta\in\mathcal{IF}_{K,p}}|\zeta|h_{K,p}\right)},$$

$\lambda^0_{K,p,\zeta}$ and $\lambda^1_{K,p}$ are given by:

$$\lambda^0_{K,p,\zeta} = \lambda_{K,p,\zeta}|K_p|h^{d-2}_{K,p} + \lambda^{\mu,0}_{K,p,\zeta}|\zeta|h_{K,p} \text{ with } \lambda^{\mu,0}_{K,p,\zeta} = \begin{cases} (1+\mu)\,|\Lambda_K \boldsymbol{n}_{K,p,\zeta}\cdot\boldsymbol{n}_{K,p,\zeta}|\gamma^{-1}_{K,p,\mu} & \text{if } \zeta \in \mathcal{IF}_{K,p}, \\ 0 & \text{otherwise,} \end{cases}$$

and

$$\lambda^1_{K,p} = \sum_{\zeta\in\mathcal{IF}_{K,p}} \gamma_1\lambda_{K,p,\zeta}|K_p| + \lambda^{\mu,1}_{K,p}|\zeta|h_{K,p} \text{ with } \lambda^{\mu,1}_{K,p,\zeta} = (1+\mu)\,\left(||\Lambda_K||_2\gamma_{K,p,\mu} + |\Lambda_K\boldsymbol{n}_{K,p,\zeta}\cdot\boldsymbol{n}_{K,p,\zeta}|\gamma^{-1}_{K,p,\mu}\right).$$

The second term of our discrete variational formulation (19):

$$-\sum_{K\in\mathcal{T}_p}\sum_{\zeta\in\mathcal{IF}_{K,p}}|\zeta|\Lambda_K\boldsymbol{W}_K\cdot\boldsymbol{n}_{K,p,\zeta}v_\zeta = -\sum_{K\in\mathcal{T}_p}\sum_{\zeta\in\mathcal{IF}_{K,p}}\int_\zeta \Lambda_K\boldsymbol{W}_K\cdot\boldsymbol{n}_{K,p,\zeta}v_\zeta,$$

expresses in fact Neumann boundary conditions on the boundary of D_p under variational form for the local problem on D_p. The coefficients $\lambda^{\mu,i}_{K,p,\zeta}$ are introduced to compensate for this term and ensure stability. The precise choice we have made for them looks quite complex and arbitrary at this point but will become completely obvious in the stability proof. For reasons that will also appear obvious later on when we will define operator $\boldsymbol{G}_K$, parameter μ can take only the two values 0 and 1, the case $\mu = 1$ corresponding to a symmetric method.

The following lemma establishes the stability properties of the local discrete variational problem (19):

Lemma 2.1. *For any $\boldsymbol{V}_p \in X_p$, we have:*

$$|K_p||\nabla\Pi_{K,p}(\boldsymbol{V}_p)|^2 \leqslant \theta_{\mathcal{F}}\theta^2_\Pi \sum_{\zeta\in\mathcal{F}_{K,p}}|K_p|h^{-2}_{K,p}|v_\zeta - v_K|^2. \tag{22}$$

Moreover there exists $\gamma^0_a > 0$ depending only on λ_*, λ^*, $\theta_{\mathcal{F}}$ and θ_Π such that for any $\boldsymbol{V}_p \in X_p$

$$a^0_p(\boldsymbol{V}_p,\boldsymbol{V}_p) \geqslant \gamma^0_a\left(\sum_{K\in\mathcal{T}_p}\sum_{\zeta\in\mathcal{F}_{K,p}}|K_p|h^{-2}_{K,p}|v_\zeta - v_K|^2\right).$$

Proof. Using Cauchy-Schwarz inequality, we get

$$|K_p||\nabla\Pi_{K,p}(\boldsymbol{V}_p)|^2 \leqslant \left(\sum_{\zeta\in\mathcal{F}_{K,p}}h^2_{K,p}|\zeta|^2|K_p|^{-2}\right)\left(\sum_{\zeta\in\mathcal{F}_{K,p}}|K_p|h^{-2}_{K,p}|v_\zeta - v_K|^2\right),$$

and we get the first result as $card(\mathcal{F}_{K,p}) \leqslant \theta_{\mathcal{F}}$. Obviously, as $\lambda^1_{K,p} \geqslant 0$ and $\lambda^{\mu,0}_{K,p,\zeta} \geqslant 0$ we have

$$a^0_p(\boldsymbol{V}_p,\boldsymbol{V}_p) \geqslant \sum_{K\in\mathcal{T}_p}\left(|K_p|\Lambda_K\nabla\Pi_{K,p}(\boldsymbol{V})\cdot\nabla\Pi_{K,p}(\boldsymbol{V}) + \sum_{\zeta\in\mathcal{F}_{K,p}}\lambda_{K,p,\zeta}|K_p|h^{-2}_{K,p}\,|v_\zeta - \Pi_{K,p}(\boldsymbol{V}_p)(\boldsymbol{x}_\zeta)|^2\right).$$

Then, using

$$(a-b)^2 \geqslant \frac{\rho}{1+\rho}a^2 - \rho\, b^2 \quad \forall\,(a,b)\in\mathbb{R}^2,\ \forall\,\rho>-1,$$

we see that, for all $\rho > -1$

$$h_{K,p}^{d-2}\,|v_\zeta - \Pi_{K,p}(\boldsymbol{V}_p)(\boldsymbol{x}_\zeta)|^2 \geqslant \frac{\rho}{1+\rho}|K_p|h_{K,p}^{-2}\,|v_\zeta - v_K|^2 - \rho|K_p|\,|\nabla\Pi_{K,p}(\boldsymbol{V}_p)|^2\,,$$

leading to, using $\lambda_* \leqslant |\lambda_{K,p,\zeta}| \leqslant \lambda^*$:

$$a_p^0(\boldsymbol{V}_p,\boldsymbol{V}_p) \geqslant \sum_{K\in\mathcal{T}_p}\left((\lambda_* - \theta_{\mathcal{F}}\rho\lambda^*)|K_p|\,|\nabla\Pi_{K,p}(\boldsymbol{V}_p)|^2 + \frac{\lambda_*\rho}{1+\rho}\sum_{\zeta\in\mathcal{F}_{K,p}}|K_p|h_{K,p}^{-2}\,|v_\zeta - v_K|^2\right),$$

and the result immediately follows with $\rho = \frac{\lambda_*}{\theta_{\mathcal{F}}\lambda^*}$ and $\gamma_a^0 = \frac{\lambda_*^2}{\theta_{\mathcal{F}}\lambda^*+\lambda_*}$. □

Immediately, noticing that for $\boldsymbol{U}_{\mathcal{T}_p} = 0$ the linear problem (19) reduces to: find $\boldsymbol{W}_p \in X_p(0)$ such that

$$a_p^0(\boldsymbol{W}_p,\boldsymbol{V}_p) = 0 \quad \forall\ \boldsymbol{V}_p \in X_p(0),$$

we deduce from lemma 2.1 that the local variational problem (19) admits a unique solution, denoted $\boldsymbol{W}_p(\boldsymbol{U}_{\mathcal{T}_p}) = (\boldsymbol{U}_{\mathcal{T}_p}, \boldsymbol{I}_p^{in}(\boldsymbol{U}_{\mathcal{T}_p}))$, defining the mappings $I_\zeta : X_{\mathcal{M}} \longmapsto \mathbb{R}$:

$$\boldsymbol{I}_p^{in}(\boldsymbol{U}_{\mathcal{T}_p}) = (I_{K,p,\zeta}(\boldsymbol{U}_{\mathcal{T}_p})_{K\in\mathcal{T}_p,\zeta\in\mathcal{F}_{K,p}} = \boldsymbol{W}_p^{in}(\boldsymbol{U}_{\mathcal{T}_p}).$$

2.1.1 Flux formulation

To define our discrete flux, let us first rewrite the bilinear form a_p. We get, after a straightforward computation:

$$a_p^0(\boldsymbol{W}_p,\boldsymbol{V}_p) = \sum_{K\in\mathcal{T}_p}\sum_{\zeta\in\mathcal{F}_{K,p}}\sum_{\zeta'\in\mathcal{F}_{K,p}}\mathbb{A}_{K,p}^{\zeta,\zeta'}(w_\zeta - w_K)(v_{\zeta'} - v_K) + \sum_{K\in\mathcal{T}_p}\sum_{\zeta\in\mathcal{F}_{K,p}}\sum_{\zeta'\in\mathcal{F}_{K,p}}\mathbb{D}_{K,p}^{\zeta,\zeta'}(w_\zeta - w_K)(v_{\zeta'} - v_K)$$

$$+ \sum_{K\in\mathcal{T}_p}\sum_{\zeta\in\mathcal{IF}_{K,p}}\sum_{i=1}^{d}\lambda_{K,p,\zeta}^1 h_{K,p}^d W_K^i V_K^i - \sum_{K\in\mathcal{T}_p}\sum_{\zeta\in\mathcal{F}_{K,p}}\sum_{i=1}^{d}\mathbb{B}_{K,p}^{i,\zeta}(W_K^i(v_\zeta - v_K) + V_K^i(w_\zeta - w_K)),$$

where

$$\left|\begin{array}{l}
\mathbb{A}_{K,p}^{\zeta,\zeta'} = \dfrac{|\zeta|\,|\zeta'|}{|K_p|}\Lambda_K\boldsymbol{n}_{K,p,\zeta}\cdot\boldsymbol{n}_{K,p,\zeta'} + y_{K,p,\zeta'}^T\mathbb{S}_{K,p}y_{K,p,\zeta},\\
\mathbb{S}_{K,p} = (\mathbb{S}_{K,p}^{\zeta,\zeta'})_{\zeta,\zeta'\in\mathcal{F}_{K,p}},\quad \mathbb{S}_{K,p}^{\zeta,\zeta'} = \delta_{\zeta,\zeta'}\lambda_{K,p,\zeta}^0,\\
y_{K,p,\zeta} = (y_{K,p}^{\zeta'})_{\zeta'\in\mathcal{F}_{K,p}},\quad y_{K,p,\zeta}^{\zeta'} = \delta_{\zeta,\zeta'} - \dfrac{|\zeta|}{|K_p|}\boldsymbol{n}_{K,p,\zeta}\cdot(\boldsymbol{x}_{\zeta'} - \boldsymbol{x}_K),\\
\mathbb{D}_{K,p}^{\zeta,\zeta'} = \lambda_{K,p}^1\dfrac{|\zeta||\zeta'|}{|K_p|^2}\boldsymbol{n}_{K,p,\zeta}\cdot\boldsymbol{n}_{K,p,\zeta'},\quad \mathbb{B}_{K,p}^{i,\zeta} = \lambda_{K,p}^1\dfrac{|\zeta|}{|K_p|}n_{K,p,\zeta}^i,
\end{array}\right.$$

with $\delta_{\zeta,\zeta'}$ is the Kronecker symbol. For any $K\in\mathcal{T}_p$ and any $\zeta\in\mathcal{F}_{K,p}$, a flux function associated to ζ is then defined by setting

$$F_{K,p}^{\zeta}(\boldsymbol{W}_p) = \sum_{\zeta'\in\mathcal{F}_{K,p}}\left(\mathbb{A}_{K,p}^{\zeta',\zeta}(w_K - w_{\zeta'}) + \mathbb{D}_{K,p}^{\zeta',\zeta}(w_K - w_{\zeta'})\right) + \sum_{i=1}^{d}\mathbb{B}_{K,p}^{i,\zeta}W_K^i, \tag{23}$$

in order to obtain, for all $\boldsymbol{V}_p \in X_p(0)$, recalling that $v_K = 0$, $\boldsymbol{V}_K = 0$ and $\boldsymbol{W}_K = \boldsymbol{U}_K$ for all $K \in \mathcal{T}$:

$$a_p(\boldsymbol{W}_p, \boldsymbol{V}_p) = -\sum_{K\in\mathcal{T}_p}\sum_{\zeta\in\mathcal{F}_{K,p}} F^{\zeta}_{K,p}(\boldsymbol{W}_p)v_\zeta - \sum_{K\in\mathcal{T}_p}\sum_{\zeta\in\mathcal{IF}_{K,p}} |\zeta|\Lambda_K\boldsymbol{U}_K\cdot\boldsymbol{n}_{K,p,\zeta'}v_\zeta = 0. \tag{24}$$

Thus, taking one degree of freedom equal to one and the others equal to zero problem (19) is equivalent to find $\boldsymbol{I}^{in}_p(\boldsymbol{U}_{\mathcal{T}_p})$ such that:

$$\left|\begin{array}{l} \displaystyle\sum_{K\in\mathcal{T}_p} F^{\zeta}_{K,p}(\boldsymbol{U}_{\mathcal{T}_p}, \boldsymbol{I}^{in}_p(\boldsymbol{U}_{\mathcal{T}_p})) = 0 \quad \text{for all } \zeta\in\mathcal{SF}_p\cap\mathcal{SF}_{in}, \\ I^{in}_\zeta(\boldsymbol{U}_{\mathcal{T}_p}) = I^{ext}_\zeta(\boldsymbol{U}^{ext}_{\mathcal{T}_p}) \quad \text{for all } \zeta\in\mathcal{SF}_p\cap\mathcal{SF}_{ext}, \\ \displaystyle F^{\zeta}_{K,p}(\boldsymbol{U}_{\mathcal{T}_p}, \boldsymbol{I}^{in}_p(\boldsymbol{U}_{\mathcal{T}_p})) = -\sum_{\zeta\in\mathcal{IF}_{K,p}} |\zeta|\Lambda_K\boldsymbol{U}_K\cdot\boldsymbol{n}_{K,p,\zeta'} \quad \text{for all } K\in\mathcal{T}_p \text{ and all } \zeta\in\mathcal{IF}_{K,p}, \end{array}\right. \tag{25}$$

which is a convenient form for solving the local variational problem in practice. This is also a much more usual form for MPFA local problems: those are formally flux continuity equations. Thus, the flux through the subface $\zeta\in\mathcal{F}_{K,p}$ for the global unknown $\boldsymbol{U}_{\mathcal{T}}$ is naturally defined by setting:

$$F^{\zeta}_{K,p}(\boldsymbol{U}_{\mathcal{T}}) = F^{\zeta}_{K,p}(\boldsymbol{U}_{\mathcal{T}_p}, \boldsymbol{I}^{in}_p(\boldsymbol{U}_{\mathcal{T}_p})), \tag{26}$$

and in particular the flux corresponding to subfaces $\zeta\in\mathcal{SF}_K\cap\mathcal{SF}_p$ appearing in the natural formulation (9) of our new MPFA method are given by:

$$F_{K,\zeta}(\boldsymbol{U}_{\mathcal{T}}) = F^{\zeta}_{K,p}(\boldsymbol{U}_{\mathcal{T}}) = F^{\zeta}_{K,p}(\boldsymbol{U}_{\mathcal{T}_p}, \boldsymbol{I}^{in}_p(\boldsymbol{U}_{\mathcal{T}_p})). \tag{27}$$

This is of course the form under which the flux are used in practice.

Remark 2.2. By construction, notice that for any subface $\zeta\in\mathcal{F}_{K,p}$:

$$F^{\zeta}_{K,p}(\boldsymbol{U}_{\mathcal{T}}) = F^{\zeta}_{K,p}(\boldsymbol{U}_{\mathcal{T}_p}, \boldsymbol{I}^{in}_p(\boldsymbol{U}_{\mathcal{T}_p})) = -|\zeta|\Lambda_K\nabla\Pi_{K,p}(\boldsymbol{U}_{\mathcal{T}_p}, \boldsymbol{I}^{in}_p(\boldsymbol{U}_{\mathcal{T}_p}))\cdot\boldsymbol{n}_{K,p,\zeta} -$$

$$\sum_{\zeta'\in\mathcal{F}_{K,p}} \lambda^0_{K,p,\zeta}\left(u_{\zeta'} - \Pi_{K,p}(\boldsymbol{U}_{\mathcal{T}_p}, \boldsymbol{I}^{in}_p(\boldsymbol{U}_{\mathcal{T}_p}))(\boldsymbol{x}_{\zeta'})\right)\left(\delta_{\zeta,\zeta'} - \frac{|\zeta|}{|K_p|}\boldsymbol{n}_{K,p,\zeta}\cdot(\boldsymbol{x}_{\zeta'} - \boldsymbol{x}_K)\right) +$$

$$\sum_{\zeta\in\mathcal{F}_{K,p}} \lambda^1_{K,p}\frac{|\zeta|}{|K_p|}\left(\boldsymbol{U}_K - \nabla\Pi_{K,p}(\boldsymbol{U}_{\mathcal{T}_p}, \boldsymbol{I}^{in}_p(\boldsymbol{U}_{\mathcal{T}_p}))\right)\cdot\boldsymbol{n}_{K,p,\zeta}, \tag{28}$$

which formally reveals the reasons why those formula correspond to consistent flux. Indeed, if $\varphi\in\mathbb{P}_1(K)$, and if one takes $u_K = \varphi(\boldsymbol{x}_K)$, $\boldsymbol{U}_K = \nabla\varphi(\boldsymbol{x}_K)$, $u_\zeta = \varphi(\boldsymbol{x}_\zeta)$, then as the operator $\Pi_{K,p}$ is exact on first order polynomials we clearly get:

$$F^{\zeta}_{K,p}(\boldsymbol{U}_{\mathcal{T}}) = -|\zeta|\Lambda_K\nabla\varphi\cdot\boldsymbol{n}_{K,p,\zeta}.$$

Our flux are thus exact on first order polynomials and it is a classical exercise to deduce their consistency.

2.1.2 The operator $\boldsymbol{G}_{\mathcal{T}}$ of the enriched MPFA method

To fully define our new MPFA method, it remains to define operator $\boldsymbol{G}_{\mathcal{T}}$. To this end, we will sum the local variational problems (19) over $p\in\mathcal{P}$, which forces us to go back to notation $v_{K,p,\zeta}$ for subfaces ζ interior to cell K, i.e.:

$$\boldsymbol{V}_p = \left((v_K, \boldsymbol{V}_K)\right)_{K\in\mathcal{T}_p}, (v_\sigma)_{\sigma\in\mathcal{F}_p\cap\mathcal{F}_{ext}}, (v_p)_{\zeta\in\mathcal{SF}_p}, (v_{K,p,\zeta})_{\zeta\in\mathcal{IF}_{K,p}}\Big).$$

Summing over $p \in \mathcal{P}$ and rearranging the sums, we immediately get:

$$\sum_{p\in\mathcal{P}} a_p(\boldsymbol{W}_p, \boldsymbol{V}_p) = \sum_{K\in\mathcal{T}} \sum_{p\in\mathcal{P}_K} |K_p|\Lambda_K \nabla\Pi_{K,p}(\boldsymbol{W}_p)\cdot\nabla\Pi_{K,p}(\boldsymbol{V}_p) + \sum_{K\in\mathcal{T}} \sum_{p\in\mathcal{P}_K} s_{K,p}(\boldsymbol{W}_p, \boldsymbol{V}_p)$$

$$- \sum_{K\in\mathcal{T}} \sum_{p\in\mathcal{P}_K} \sum_{\zeta\in\mathcal{IF}_{K,p}} |\zeta|\Lambda_K \boldsymbol{W}_K\cdot\boldsymbol{n}_{K,p,\zeta} v_{K,p,\zeta},$$

which is a bilinear form on the space $X_0 = X_{\mathcal{T},0}\times X^{in}$. Using our parameter $\mu \in \{0,1\}$ introduced in our stability coefficient to enforce symmetry if desired, we slightly modify the above expression to finally define a global bilinear form a_h by setting for all $(\boldsymbol{W},\boldsymbol{V}) \in X_0\times X_0$:

$$a_h(\boldsymbol{W}, \boldsymbol{V}) = \sum_{K\in\mathcal{T}} \sum_{p\in\mathcal{P}_K} |K_p|\Lambda_K \nabla\Pi_{K,p}(\boldsymbol{W}_p)\cdot\nabla\Pi_{K,p}(\boldsymbol{V}_p) + \sum_{K\in\mathcal{T}} \sum_{p\in\mathcal{P}_K} s_{K,p}(\boldsymbol{W}_p, \boldsymbol{V}_p)$$

$$- \sum_{K\in\mathcal{T}} \sum_{p\in\mathcal{P}_K} \sum_{\zeta\in\mathcal{IF}_{K,p}} |\zeta|\Lambda_K \boldsymbol{W}_K\cdot\boldsymbol{n}_{K,p,\zeta} v_{K,p,\zeta} - \mu \sum_{K\in\mathcal{T}} \sum_{p\in\mathcal{P}_K} \sum_{\zeta\in\mathcal{IF}_{K,p}} |\zeta|\Lambda_K \boldsymbol{V}_K\cdot\boldsymbol{n}_{K,p,\zeta} w_{K,p,\zeta}. \tag{29}$$

We see that a_h is indeed symmetric if $\mu = 1$, and is non-symmetric if $\mu = 0$ although more natural starting from the local variational problems. As (29) is clearly a discrete counterpart of the bilinear form induced by model problem (1)-(2), we naturally consider the global variational formulation find $\boldsymbol{U} \in X_0$ such that

$$a_h(\boldsymbol{U},\boldsymbol{V}) = l_h(\boldsymbol{V}) \quad \forall\, \boldsymbol{V}\in X_0 \quad \text{with} \quad l_h(\boldsymbol{V}) = \sum_{K\in\mathcal{T}} |K| f_K v_K. \tag{30}$$

It is now easy to establish the following equivalence result:

Theorem 2.3. *For any $\mu \in \{0,1\}$, solving (30) is equivalent to solving the generic MPFA problem (9) with operators $\boldsymbol{I}^{in}$ and $(F_{K,p})_{K\in\mathcal{T},\zeta\in\mathcal{SF}_K}$ given by the local problems (25) and with operator $\boldsymbol{G}_{\mathcal{T}}$ defined by:*

$$\boldsymbol{G}_K(\boldsymbol{U}_{\mathcal{T}}) = \frac{1}{\lambda_K^G} \sum_{p\in\mathcal{P}_K} \left(\lambda^1_{K,p} \nabla\Pi_{K,p}(\boldsymbol{U}_{\mathcal{T}_p}, \boldsymbol{I}_p^{in}(\boldsymbol{U}_{\mathcal{T}_p})) + \mu \sum_{\zeta\in\mathcal{IF}_{K,p}} |\zeta| I_{K,p,\zeta}(\boldsymbol{U}_{\mathcal{T}_p}) \Lambda_K^T \boldsymbol{n}_{K,p,\zeta} \right), \tag{31}$$

where $\lambda_K^G = \sum_{p\in\mathcal{P}_K} \lambda^1_{K,p} > 0$.

Proof. The proof is in fact elementary and simply consists in correctly choosing test functions to make the local problems appear. For any $p\in\mathcal{P}$ and any $\boldsymbol{V}_p \in X_p(0)$, let $\hat{\boldsymbol{V}}\in X_0$ be such that $\hat{\boldsymbol{V}}_p = \boldsymbol{V}_p$, $\hat{\boldsymbol{V}}_{p'} = 0$ for all $p' \neq p$. Using such a $\hat{\boldsymbol{V}}$, we immediately see that $a_{p'}(\boldsymbol{W},\hat{\boldsymbol{V}}) = 0$ for all $p'\in\mathcal{P}$, $p'\neq p$, as well as $l_h(\hat{\boldsymbol{V}}) = 0$ and

$$-\mu \sum_{K\in\mathcal{T}} \sum_{p\in\mathcal{P}_K} \sum_{\zeta\in\mathcal{IF}_{K,p}} |\zeta|\Lambda_K \hat{\boldsymbol{V}}_K\cdot\boldsymbol{n}_{K,p,\zeta} w_{K,p,\zeta} = 0,$$

as $\hat{\boldsymbol{V}}_K = 0$ for all $K\in\mathcal{T}$. Thus we clearly have, if $\boldsymbol{U}$ is solution of (30):

$$a_h(\boldsymbol{U},\hat{\boldsymbol{V}}) = a_p(\boldsymbol{U}_p,\boldsymbol{V}_p) = \sum_{K\in\mathcal{T}_p} |K_p|\Lambda_K \nabla\Pi_{K,p}(\boldsymbol{W}_p)\cdot\nabla\Pi_{K,p}(\boldsymbol{V}_p) + \sum_{K\in\mathcal{T}_p} s_{K,p}(\boldsymbol{W}_p,\boldsymbol{V}_p)$$

$$- \sum_{K\in\mathcal{T}_p} \sum_{\zeta\in\mathcal{IF}_{K,p}} |\zeta|\Lambda_K \boldsymbol{W}_K\cdot\boldsymbol{n}_{K,p,\zeta} v_{K,p,\zeta} = 0 \quad \forall\, \boldsymbol{V}_p\in X_p(0),$$

implying that $\boldsymbol{U}_p$ is the unique solution to the local variational problem (25) and thus $\boldsymbol{U}_p = (\boldsymbol{U}_{\mathcal{T}_p}, \boldsymbol{I}_p(\boldsymbol{U}_p))$. Next, for some $K\in\mathcal{T}$ and some $1\leqslant i\leqslant d$, taking $V_K^i = 1$ in the global variational formulation and all others degrees of freedom of $\boldsymbol{V}$ equal to zero, we get:

$$\sum_{p\in\mathcal{P}_K} \lambda^1_{K,p}(U_K^i - \nabla\Pi_{K,p}(\boldsymbol{U}_p)\cdot\boldsymbol{e}_i) - \mu \sum_{p\in\mathcal{P}_K} \sum_{\zeta\in\mathcal{IF}_{K,p}} |\zeta|\Lambda_K^T \boldsymbol{n}_{K,p,\zeta}\cdot\boldsymbol{e}_i u_{K,p,\zeta} = 0,$$

and thus we do obtain $\boldsymbol{U}_K = \boldsymbol{G}_K(\boldsymbol{U}_\mathcal{T})$, with $\boldsymbol{G}_K$ defined by (31). Finally, we have by construction:

$$a_h(\boldsymbol{U},\boldsymbol{V}) = \sum_{p\in\mathcal{P}} a_p(\boldsymbol{U}_p,\boldsymbol{V}_p) - \mu \sum_{K\in\mathcal{T}} \sum_{p\in\mathcal{P}_K} \sum_{\zeta\in\mathcal{IF}_{K,p}} |\zeta|\Lambda_K \boldsymbol{V}_K\cdot\boldsymbol{n}_{K,p,\zeta} u_{K,p,\zeta}$$

$$= \sum_{p\in\mathcal{P}} \sum_{K\in\mathcal{T}_p} \sum_{\zeta\in\mathcal{F}_{K,p}} F^\zeta_{K,p}(\boldsymbol{U}_p)(v_K - v_{K,p,\zeta}) - \sum_{K\in\mathcal{T}_p} \sum_{\zeta\in\mathcal{IF}_{K,p}} |\zeta|\Lambda_K \boldsymbol{U}_K\cdot\boldsymbol{n}_{K,p,\zeta} v_{K,p,\zeta}$$

$$-\mu \sum_{K\in\mathcal{T}} \sum_{p\in\mathcal{P}_K} \sum_{\zeta\in\mathcal{IF}_{K,p}} |\zeta|\Lambda_K \boldsymbol{V}_K\cdot\boldsymbol{n}_{K,p,\zeta} u_{K,p,\zeta}.$$

Taking $v_K = 1$ for some $K\in\mathcal{T}$ and all others degrees of freedom of $\boldsymbol{V}$ equal to zero, we deduce from (30) that:

$$\sum_{p\in\mathcal{P}_K} \sum_{\zeta\in\mathcal{F}_{K,p}} F^\zeta_{K,p}(\boldsymbol{U}_p) = |K| f_K.$$

However as we know that $\boldsymbol{U}_p$ is solution of the local flux continuity problem:

$$\sum_{p\in\mathcal{P}_K} \sum_{\zeta\in\mathcal{F}_{K,p}} F^\zeta_{K,p}(\boldsymbol{U}_p) = \sum_{p\in\mathcal{P}_K} \sum_{\zeta\in\mathcal{SF}_{K,p}} F^\zeta_{K,p}(\boldsymbol{U}_p) + \sum_{p\in\mathcal{P}_K} \sum_{\zeta\in\mathcal{IF}_{K,p}} F^\zeta_{K,p}(\boldsymbol{U}_p)$$

$$= \sum_{p\in\mathcal{P}_K} \sum_{\zeta\in\mathcal{SF}_{K,p}} F^\zeta_{K,p}(\boldsymbol{U}_p) - \sum_{p\in\mathcal{P}_K} \sum_{\zeta\in\mathcal{IF}_{K,p}} |\zeta|\Lambda_K \boldsymbol{U}_K\cdot\boldsymbol{n}_{K,p,\zeta}.$$

But we clearly have:

$$-\sum_{p\in\mathcal{P}_K} \sum_{\zeta\in\mathcal{IF}_{K,p}} |\zeta|\Lambda_K \boldsymbol{U}_K\cdot\boldsymbol{n}_{K,p,\zeta''} = -\sum_{\zeta\in\mathcal{IF}_K} |\zeta|\Lambda_K \boldsymbol{U}_K\cdot\left(\sum_{p\in\mathcal{P}_K \mid \zeta\in\mathcal{IF}_{K,p}} \boldsymbol{n}_{K,p,\zeta}\right) = 0,$$

and we thus recover:

$$\sum_{p\in\mathcal{P}_K} \sum_{\zeta\in\mathcal{SF}_{K,p}} F^\zeta_{K,p}(\boldsymbol{U}_p) = \sum_{\zeta\in\mathcal{SF}_K} F_{K,\zeta}(\boldsymbol{U}_p) = |K| f_K.$$

Thus, we have established that a solution of (30) is indeed solution of the generic MPFA problem (9) with the announced choices for operators $\boldsymbol{I}^{in}$ and $(F_{K,p})_{K\in\mathcal{T},p\in\mathcal{P}_K}$ and $\boldsymbol{G}_\mathcal{T}$. As we have in fact covered all the possibilities for the test function $\boldsymbol{V}$ it is immediate to see that the converse holds true, which concludes the proof. □

In practice, it is useful to notice that multiplying equation $\boldsymbol{U}_K = \boldsymbol{G}_K(\boldsymbol{U}_\mathcal{T})$ by λ^G_K we get:

$$0 = \lambda^G_K \boldsymbol{U}_K - \lambda^G_K \boldsymbol{G}_K(\boldsymbol{U}_\mathcal{T}) = \sum_{p\in\mathcal{P}_K} \boldsymbol{G}_{K,p}(\boldsymbol{U}_\mathcal{T}),$$

where

$$\boldsymbol{G}_{K,p}(\boldsymbol{U}_\mathcal{T}) = \lambda^1_{K,p}\left(\boldsymbol{U}_K - \nabla\Pi_{K,p}(\boldsymbol{U}_{\mathcal{T}_p}, \boldsymbol{I}^{in}_p(\boldsymbol{U}_{\mathcal{T}_p}))\right) - \mu \sum_{\zeta\in\mathcal{IF}_{K,p}} |\zeta| I_{K,p,\zeta}(\boldsymbol{U}_{\mathcal{T}_p}) \Lambda^T_K \boldsymbol{n}_{K,p,\zeta}, \tag{32}$$

which was in fact the expression from which we have deduced the precise form of $\boldsymbol{G}_K(\boldsymbol{U}_\mathcal{T})$ in the above proof. Computing each $\boldsymbol{G}_{K,p}(\boldsymbol{U}_\mathcal{T})$ instead of $\boldsymbol{G}_K(\boldsymbol{U}_\mathcal{T})$ will indeed lead to a much easier implementation of the method, as we can handle them in flux-like assembling loops (see subsection 2.2).

Finally, let us observe that the stencil of the cell equations $\sum_{\zeta\in\mathcal{SF}_K} F_{K,\zeta}(\boldsymbol{U}_\mathcal{T}, \boldsymbol{U}^{in}) = |K| f_K$ and $\boldsymbol{U}_K = \boldsymbol{G}_K(\boldsymbol{U}_\mathcal{T})$ for cell K simply correspond to the cell unknowns of cell belonging to $\cup_{p\in\mathcal{P}_K}\mathcal{T}_p$. This implies that for the face and subface based subdomains, the stencil of the resulting enriched MPFA methods for a given cell K consists in the cells that are immediate neighbours through faces of cell K, or in other words it leads to the same stencil as the TPFA scheme. For the O shaped domains, the corresponding enriched MPFA has this time the same stencil has the MPFAO scheme, i.e. neighbours through vertices. In any case the enriched MPFA methods do have a compact stencil as claimed in the introduction.

Remark 2.4. The final formulation is very reminiscent of incomplete interior penalty (IIP) discontinuous Galerkin method for $\mu = 0$ and symmetric interior penalty (SIP) discontinuous Galerkin method for $\mu = 1$ (see [28, 29]). Indeed, roughly speaking we recognize in (29) the four terms of SIP dG methods: the symmetric bilinear form on gradients, the two flux terms on some boundaries, and a stabilization part. However, a closer look makes it obvious that there are also many differences: our boundary flux terms are not on the boundary of the cell, but on some internal boundaries (in this sense, it could also be compared to a discontinuous Galerkin method on the submesh $\mathcal{SM}$ rather that on the mesh itself, but for which jumps are not allowed only on faces interior to the cells of the original mesh). The stabilization term does not involve jumps on the boundaries of the cell as we enforce trace continuity on subfaces, but rather two different ways of expressing consistency. Finally we do not use the gradient unknowns to approximate the diffusion operators, for which gradient reconstructions based on subfaces unknowns are preferred. We only resort to the gradient unknowns to enforce flux continuity in the interior of the cells of the original mesh. Nevertheless it is interesting to notice the formal resemblance (in particular to establish convergence) as well as the fact that once the intermediate unknowns are eliminated, our new MPFA methods has the same number $(d + 1)$ of degrees of freedom per cell than first order discontinuous Galerkin methods on the original mesh $\mathcal{M}$ (and not on the submesh $\mathcal{SM}$).

2.2 Implementation details

The implementation of the enriched MPFA methods follows the usual lines of the MPFA methods. In a sequential setting, the most efficient assembling procedure should loop over the partitioning set $\mathcal{P}$ to solve the local problems once and use their solution to update the cell equations for cells $K \in \mathcal{T}_p$. In a shared memory setting, an alternative (with storage) would consist in again looping over the set $\mathcal{P}$ to compute the local flux operators and gradient operator contributions, but instead of immediately updating the cell equations postpone it to a second loop over cells (see algorithm 1). In this way, no concurrent write access to cell equations is needed, the only concurrency being potential simultaneous but non locking read access to the stored flux and gradient operators (without storage, this second version implies recomputing the flux and gradient operators several times to avoid locking write access).

Algorithm 1 Pseudo code for assembling the enriched MPFA methods

Initialization:
for $p \in \mathcal{P}$ **do**
  Compute the local domain D_p and its geometric properties.
  for $K \in \mathcal{T}_p$ **do**
    Compute the local flux $F^{\zeta}_{K,p}$ for $\zeta \in \mathcal{F}_{K,p}$ using (23).
  end for
  Solve the local variational problem under flux form (25) and deduce the operators $\boldsymbol{I}^{in}_p$.
  Compute the local "cell-centered" flux $(F_{K,\zeta})_{K\in\mathcal{T}_p,\zeta\in\mathcal{SF}_{K,p}}$ using formula (27) : $F_{K,\zeta}(\boldsymbol{U}_{\mathcal{T}}) = F^{\zeta}_{K,p}(\boldsymbol{U}_{\mathcal{T}_p}, \boldsymbol{I}^{in}_p(\boldsymbol{U}_{\mathcal{T}_p}))$ and the gradient operator contributions $(\boldsymbol{G}_{K,p})_{K\in\mathcal{T}_p}$ using (32), and store them.
end for
Assembly loop:
for $K \in \mathcal{T}$ **do**
  for $p \in \mathcal{P}_K$ **do**
    Get the "cell-centered" flux $(F_{K,\zeta})_{K\in\mathcal{T}_p,\zeta\in\mathcal{SF}_{K,p}}$ and the gradient operator contributions $(\boldsymbol{G}_{K,p})_{K\in\mathcal{T}_p}$ and add their contributions to the cell equations $\sum_{\zeta\in\mathcal{SF}_K} F_{K,\zeta}(\boldsymbol{U}_{\mathcal{T}}, \boldsymbol{U}^{in}) = |K| f_K$ and $\boldsymbol{U}_K = \boldsymbol{G}_K(\boldsymbol{U}_{\mathcal{T}})$.
  end for
end for
for $\sigma \in \mathcal{F}_{ext}$ **do**
  Enforce the Dirichlet boundary conditions $u_\sigma = 0$
end for

2.3 Stability of the enriched MPFA methods

So far, we have only established the well-posedness of the local problems. Fortunately, we have also derived an equivalent global variational formulation from which it is easy to deduce the stability of the overall MPFA method. To this end, we define the scalar product

$$(\boldsymbol{W},\boldsymbol{V})_{X,1} = \sum_{K\in\mathcal{T}}\sum_{p\in\mathcal{P}_K}\sum_{\zeta\in\mathcal{F}_{K,p}} |K_p| h_K^{-2}(w_{K,p,\zeta}-w_K)(v_{K,p,\zeta}-v_K) +$$

$$\sum_{K\in\mathcal{T}}\sum_{p\in\mathcal{P}_K} |K_p|(\boldsymbol{W}_K - \nabla\Pi_{K,p}(\boldsymbol{W}))\cdot(\boldsymbol{V}_K - \nabla\Pi_{K,p}(\boldsymbol{V})) \quad \forall\,(\boldsymbol{W},\boldsymbol{V})\in X_0\times X_0,$$

and the associated semi-norm

$$|\boldsymbol{V}|_{X,1}^2 = \sum_{K\in\mathcal{T}}\sum_{p\in\mathcal{P}_K}\sum_{\zeta\in\mathcal{F}_{K,p}} |K_p| h_{K,p}^{-2}|v_{K,p,\zeta}-v_K|^2 + \sum_{K\in\mathcal{T}}\sum_{p\in\mathcal{P}_K} |K_p||\boldsymbol{V}_K - \nabla\Pi_{K,p}(\boldsymbol{V}))|^2 \quad \boldsymbol{V}\in X_0,$$

which is clearly a norm on X_0 . Notice that we have made a slight abuse of notations for subfaces $\zeta\in\mathcal{SF}$ by denoting $v_{K,p,\zeta}=v_\zeta$ if $\zeta\in\mathcal{SF}_K\cap\mathcal{SF}_p$, allowing more compact notations. Establishing stability now roughly speaking consists in noticing that we have correctly chosen the values of $\lambda^{\mu,0}_{K,p,\zeta}$ and $\lambda^{\mu,1}_{K,p,\zeta}$ to compensate for the boundary terms, leading to:

Theorem 2.5. *There exists $C_a>0$ and $\gamma_a>0$ independent on h but depending on d, λ_*, λ^*, $\theta_{\mathcal{F}}$, θ_Π and $\theta_{\mathcal{P}}$ such that such that for any $(\boldsymbol{W},\boldsymbol{V})\in X_0\times X_0$:*

$$a_h(\boldsymbol{W},\boldsymbol{V}) \leqslant C_a|\boldsymbol{W}|_{X,1}|\boldsymbol{V}|_{X,1} \quad \text{and} \quad a_h(\boldsymbol{V},\boldsymbol{V}) \geqslant \gamma_a|\boldsymbol{V}|_{X,1}^2. \tag{33}$$

Proof. We have by definition:

$$a_h(\boldsymbol{V},\boldsymbol{V}) = \sum_{K\in\mathcal{T}}\sum_{p\in\mathcal{P}_K} |K_p|\Lambda_K\nabla\Pi_{K,p}(\boldsymbol{V}_p)\cdot\nabla\Pi_{K,p}(\boldsymbol{V}_p) + \sum_{K\in\mathcal{T}}\sum_{p\in\mathcal{P}_K} s_{K,p}(\boldsymbol{V}_p,\boldsymbol{V}_p)$$

$$-(1+\mu)\sum_{K\in\mathcal{T}}\sum_{p\in\mathcal{P}_K}\sum_{\zeta\in\mathcal{IF}_{K,p}} |\zeta|\Lambda_K\boldsymbol{V}_K\cdot\boldsymbol{n}_{K,p,\zeta}v_{K,p,\zeta} = T_1+T_2+T_3,$$

with obvious notations. Using $\sum_{p\in\mathcal{P}_K\ |\ \zeta\in\mathcal{IF}_{K,p}}\boldsymbol{n}_{K,p,\zeta}=0$ for any $\zeta\in\mathcal{IF}_K$, we get

$$\sum_{K\in\mathcal{T}}\sum_{p\in\mathcal{P}_K}\sum_{\zeta\in\mathcal{IF}_{K,p}} |\zeta|\Lambda_K\boldsymbol{V}_K\cdot\boldsymbol{n}_{K,p,\zeta}\left(v_K+\boldsymbol{V}_K\cdot(\boldsymbol{x}_\zeta-\boldsymbol{x}_K)\right)=0.$$

The last term T_3 thus rewrites:

$$T_3 = -(1+\mu)\sum_{K\in\mathcal{T}}\sum_{p\in\mathcal{P}_K}\sum_{\zeta\in\mathcal{IF}_{K,p}} |\zeta|\Lambda_K\boldsymbol{V}_K\cdot\boldsymbol{n}_{K,p,\zeta}\left(v_{K,p,\zeta}-v_K-\boldsymbol{V}_K\cdot(\boldsymbol{x}_\zeta-\boldsymbol{x}_K)\right)$$

$$= -(1+\mu)\sum_{K\in\mathcal{T}}\sum_{p\in\mathcal{P}_K}\sum_{\zeta\in\mathcal{IF}_{K,p}} |\zeta|\Lambda_K\boldsymbol{V}_K\cdot\boldsymbol{n}_{K,p,\zeta}R_{K,p,\zeta}(\boldsymbol{V}),$$

where we have denoted

$$R_{K,p,\zeta}(\boldsymbol{V}) = v_{K,p,\zeta}-v_K-\nabla\Pi_{K,p}(\boldsymbol{V})\cdot(\boldsymbol{x}_\zeta-\boldsymbol{x}_K)-(\boldsymbol{V}_K-\nabla\Pi_{K,p}(\boldsymbol{V}))\cdot(\boldsymbol{x}_\zeta-\boldsymbol{x}_K).$$

To establish stability, we need to estimate T_3 carefully. We get for $\gamma_{K,p,\mu}>0$:

$$-|\zeta|\Lambda_K\boldsymbol{V}_K\cdot\boldsymbol{n}_{K,p,\zeta}R_{K,p,\zeta}(\boldsymbol{V}) \geqslant -\gamma_{K,p,\mu}|\zeta|h_{K,p}\left(\gamma_{K,p,\mu}^{-1}h_{K,p}^{-1}|\Lambda_K\boldsymbol{V}_K\cdot\boldsymbol{n}_{K,p,\zeta}R_{K,p,\zeta}(\boldsymbol{V})|\right)$$

$$\geqslant -\frac{\gamma_{K,p,\mu} h_{K,p} |\zeta|}{2} \left(h_{K,p}^{-2} \gamma_{K,p,\mu}^{-2} |\Lambda_K \boldsymbol{n}_{K,p,\zeta} \cdot \boldsymbol{n}_{K,p,\zeta}| |R_{K,p,\zeta}(\boldsymbol{V})|^2 + |\Lambda_K \boldsymbol{V}_K \cdot \boldsymbol{V}_K| \right).$$

Then

$$|\Lambda \boldsymbol{V}_K \cdot \boldsymbol{V}_K|^2 \leqslant 2|\Lambda_K(\boldsymbol{V}_K - \nabla \Pi_{K,p}(\boldsymbol{V})) \cdot (\boldsymbol{V}_K - \nabla \Pi_{K,p}(\boldsymbol{V}))| + 2|\Lambda_K \nabla \Pi_{K,p}(\boldsymbol{V}) \cdot \nabla \Pi_{K,p}(\boldsymbol{V})|,$$

and

$$|R_{K,p,\zeta}(\boldsymbol{V})|^2 \leqslant 2|v_{K,p,\zeta} - v_K - \nabla \Pi_{K,p}(\boldsymbol{V}) \cdot (\boldsymbol{x}_\zeta - \boldsymbol{x}_K)|^2 + 2h_{K,p}^2 |\boldsymbol{V}_K - \nabla \Pi_{K,p}(\boldsymbol{V})|^2,$$

finally lead to:

$$-|\zeta| \Lambda_K \boldsymbol{V}_K \cdot \boldsymbol{n}_{K,p,\zeta} R_{K,p,\zeta}(\boldsymbol{V}) \geqslant -\gamma_{K,p,\mu}^{-1} h_{K,p}^{-1} |\zeta| \, |\Lambda_K \boldsymbol{n}_{K,p,\zeta} \cdot \boldsymbol{n}_{K,p,\zeta}| \, |v_{K,p,\zeta} - v_K - \nabla \Pi_{K,p}(\boldsymbol{V}) \cdot (\boldsymbol{x}_\zeta - \boldsymbol{x}_K)|^2$$

$$-h_{K,p} \gamma_{K,p,\mu}^{-1} |\zeta| \, |\Lambda_K \boldsymbol{n}_{K,p,\zeta} \cdot \boldsymbol{n}_{K,p,\zeta}| \boldsymbol{V}_K - \nabla \Pi_{K,p}(\boldsymbol{V})|^2 - h_{K,p} \gamma_{K,p,\mu} |\zeta| \, |\Lambda_K (\boldsymbol{V}_K - \nabla \Pi_{K,p}(\boldsymbol{V})) \cdot (\boldsymbol{V}_K - \nabla \Pi_{K,p}(\boldsymbol{V}))|$$
$$-\gamma_{K,p,\mu} h_{K,p} |\zeta| \, |\Lambda_K \nabla \Pi_{K,p}(\boldsymbol{V}) \cdot \nabla \Pi_{K,p}(\boldsymbol{V})|.$$

We finally obtain:

$$T_3 \geqslant -(1+\mu) \sum_{K \in \mathcal{T}} \sum_{p \in \mathcal{P}_K} \sum_{\zeta \in \mathcal{IF}_{K,p}} \left(\gamma_{K,p,\mu}^{-1} |\zeta| h_{K,p}^{-1} |\Lambda_K \boldsymbol{n}_{K,p,\zeta} \cdot \boldsymbol{n}_{K,p,\zeta}| \, |v_{K,p,\zeta} - v_K - \nabla \Pi_{K,p}(\boldsymbol{V}) \cdot (\boldsymbol{x}_\zeta - \boldsymbol{x}_K)|^2 \right.$$

$$+|\zeta| h_{K,p} \left(\gamma_{K,p,\mu} ||\Lambda_K||_2 + \gamma_{K,p,\mu}^{-1} \, |\Lambda_K \boldsymbol{n}_{K,p,\zeta} \cdot \boldsymbol{n}_{K,p,\zeta} \right) |\boldsymbol{V}_K - \nabla \Pi_{K,p}(\boldsymbol{V})|^2$$
$$\left. +|\zeta| h_{K,p} \gamma_{K,p,\mu} |\Lambda_K \nabla \Pi_{K,p}(\boldsymbol{V}) \cdot \nabla \Pi_{K,p}(\boldsymbol{V})| \right).$$

Recalling that:

$$\lambda_{K,p,\zeta}^{\mu,0} = \begin{cases} (1+\mu) \, |\Lambda_K \boldsymbol{n}_{K,p,\zeta} \cdot \boldsymbol{n}_{K,p,\zeta}| \gamma_{K,p,\mu}^{-1} & \text{if } \zeta \in \mathcal{IF}_{K,p}, \\ 0 & \text{otherwise,} \end{cases}$$

and

$$\lambda_{K,p,\zeta}^{\mu,1} = (1+\mu) \, \left(||\Lambda_K||_2 \gamma_{K,p,\mu} + |\Lambda_K \boldsymbol{n}_{K,p,\zeta} \cdot \boldsymbol{n}_{K,p,\zeta}| \gamma_{K,p,\mu}^{-1} \right),$$

we see that the two first terms are precisely the opposite of the additional terms involving $\lambda_{K,p,\zeta}^{\mu,i}$ in the stabilization form s_p. Thus, proceeding as in the proof of lemma 2.1, we see that

$$|K_p| h_{K,p}^{-2} \, |v_\zeta - \Pi_{K,p}(\boldsymbol{V}_p)(\boldsymbol{x}_\zeta)|^2 \geqslant \frac{\rho}{1+\rho} |K_p| h_{K,p}^{-2} \, |v_\zeta - v_K|^2 - \rho |K_p| \, |\nabla \Pi_{K,p}(\boldsymbol{V}_p)|^2,$$

leads to, as $\lambda_* \leqslant \lambda_{K,p,\zeta} \leqslant \lambda^*$:

$$T_2 + T_3 \geqslant \sum_{K \in \mathcal{T}} \sum_{p \in \mathcal{P}_K} \left(-(1+\mu) \gamma_{K,p,\mu} \left(\sum_{\zeta \in \mathcal{IF}_{K,p}} |\zeta| h_{K,p} \right) \Lambda_K \nabla \Pi_{K,p}(\boldsymbol{V}_p) \cdot \nabla \Pi_{K,p}(\boldsymbol{V}_p) + \right.$$

$$\left. -card(\mathcal{F}_{K,p}) \rho \lambda^* |K_p| \, |\nabla \Pi_{K,p}(\boldsymbol{V}_p)|^2 + \frac{\lambda_* \rho}{1+\rho} \sum_{\zeta \in \mathcal{F}_{K,p}} |K_p| h_{K,p}^{-2} \, |v_{K,p,\zeta} - v_K|^2 + \gamma_1 \lambda_* |K_p| |\boldsymbol{V}_K - \nabla \Pi_{K,p}(\boldsymbol{V}_p)|^2 \right),$$

and consequently, for any $0 < \gamma_0 < 1$:

$$a_h(\boldsymbol{V}, \boldsymbol{V}) \geqslant \sum_{K \in \mathcal{T}} \sum_{p \in \mathcal{P}_K} \left(\left(\gamma_0 |K_p| - (1+\mu) \gamma_{K,p,\mu} \left(\sum_{\zeta \in \mathcal{IF}_{K,p}} |\zeta| h_{K,p} \right) \right) \Lambda_K \nabla \Pi_{K,p}(\boldsymbol{V}) \cdot \nabla \Pi_{K,p}(\boldsymbol{V}) + \right.$$

$$\left((1-\gamma_0)\lambda_* - \theta_{\mathcal{F}}\rho\lambda^*\right)|K_p|\,|\nabla\Pi_{K,p}(\boldsymbol{V}_p)|^2 + \frac{\lambda_*\rho}{1+\rho}\sum_{\zeta\in\mathcal{F}_{K,p}}|K_p|h_{K,p}^{-2}\,|v_\zeta - v_K|^2 + \gamma_1\lambda_*|K_p||\boldsymbol{V}_K - \nabla\Pi_{K,p}(\boldsymbol{V}_p)|^2\Bigg),$$

and the coercivity result immediately follows with

$$\rho = \frac{(1-\gamma_0)\lambda_*}{\theta_{\mathcal{F}}\lambda^*} \quad \text{and} \quad \gamma_a^0 = \min\left(\gamma_1\lambda_*, \frac{(1-\gamma_0)\lambda_*^2}{\theta_{\mathcal{F}}\lambda^* + (1-\gamma_0)\lambda_*}\right) \quad \text{as} \quad \gamma_{K,p,\mu} = \frac{\gamma_0|K_p|}{(1+\mu)\left(\sum_{\zeta\in\mathcal{IF}_{K,p}}|\zeta|h_{K,p}\right)}.$$

To establish boundedness, recall that by definition:

$$a_h(\boldsymbol{W},\boldsymbol{V}) = \sum_{K\in\mathcal{T}}\sum_{p\in\mathcal{P}_K}|K_p|\Lambda_K\nabla\Pi_{K,p}(\boldsymbol{W}_p)\cdot\nabla\Pi_{K,p}(\boldsymbol{V}_p) + \sum_{K\in\mathcal{T}}\sum_{p\in\mathcal{P}_K}s_{K,p}(\boldsymbol{W}_p,\boldsymbol{V}_p)$$

$$-\sum_{K\in\mathcal{T}}\sum_{p\in\mathcal{P}_K}\sum_{\zeta\in\mathcal{IF}_{K,p}}|\zeta|\Lambda_K\boldsymbol{W}_K\cdot\boldsymbol{n}_{K,p,\zeta}v_{K,p,\zeta} - \mu\sum_{K\in\mathcal{T}}\sum_{p\in\mathcal{P}_K}\sum_{\zeta\in\mathcal{IF}_{K,p}}|\zeta|\Lambda_K\boldsymbol{V}_K\cdot\boldsymbol{n}_{K,p,\zeta}w_{K,p,\zeta} = T_1+T_2+T_3+T_4.$$

The treatment of the two boundary terms being identical we only detail the first one. Again, as by construction, we have:

$$\sum_{p\in\mathcal{P}_K}\sum_{\zeta\in\mathcal{IF}_{K,p}}|\zeta|\Lambda_K\boldsymbol{W}_K\cdot\boldsymbol{n}_{K,p,\zeta}v_K = 0,$$

using Cauchy-Schwarz inequality and $|\zeta|\leqslant h_{K,p}^{d-1}$ we can write:

$$\left|\sum_{K\in\mathcal{T}}\sum_{p\in\mathcal{P}_K}\sum_{\zeta\in\mathcal{IF}_{K,p}}|\zeta|\Lambda_K\boldsymbol{W}_K\cdot\boldsymbol{n}_{K,p,\zeta}v_{K,p,\zeta}\right|$$

$$\leqslant\theta_\Pi\lambda^*\left(\sum_{K\in\mathcal{T}}\sum_{p\in\mathcal{P}_K}\sum_{\zeta\in\mathcal{IF}_{K,p}}|K_p||\boldsymbol{W}_K|^2\right)^{1/2}\left(\sum_{K\in\mathcal{T}}\sum_{p\in\mathcal{P}_K}\sum_{\zeta\in\mathcal{IF}_{K,p}}|K_p|h_{K,p}^{-2}|v_{K,p,\zeta}-v_K|^2\right)^{1/2}.$$

Next, we have for any $\zeta\in\mathcal{F}_{K,p}$:

$$|K_p|h_{K,p}^{-2}\,|v_\zeta - \Pi_{K,p}(\boldsymbol{V}_p)(\boldsymbol{x}_\zeta)|^2 \leqslant 2|K_p|h_{K,p}^{-2}\,|v_\zeta - v_K|^2 + 2|K_p|h_{K,p}^{-2}\,|\nabla\Pi_{K,p}(\boldsymbol{V}_p)\cdot(\boldsymbol{x}_\zeta-\boldsymbol{x}_K)|^2$$

$$\leqslant 2|K_p|h_{K,p}^{-2}\,|v_\zeta - v_K|^2 + 2|K_p|\,|\nabla\Pi_{K,p}(\boldsymbol{V}_p)|^2.$$

As

$$\frac{\gamma_0\theta_\Pi^{-1}}{2\theta_{\mathcal{F}}}\leqslant\gamma_{K,p,\mu}\leqslant\gamma_0\theta_\Pi \quad \text{for} \quad \gamma_{K,p,\mu} = \frac{\gamma_0|K_p|}{(1+\mu)\left(\sum_{\zeta\in\mathcal{IF}_{K,p}}|\zeta|h_{K,p}\right)},$$

we see that

$$|\lambda_{K,p,\zeta}|\leqslant\lambda^* \quad \text{and} \quad \lambda_{K,p,\zeta}^{\mu,0}\leqslant 4\lambda^*\theta_\Pi\theta_{\mathcal{F}}\gamma_0^{-1} \quad \text{and} \quad \lambda_{K,p,\zeta}^{\mu,1}\leqslant 2\lambda^*\theta_\Pi\left(\gamma_0+2\theta_{\mathcal{F}}\gamma_0^{-1}\right),$$

and thus using again Cauchy-Schwarz inequality we get that for some $C>0$ independent on h

$$T_1+T_2\leqslant C\sum_{K\in\mathcal{T}}\sum_{p\in\mathcal{P}_K}|K_p|\,|\nabla\Pi_{K,p}(\boldsymbol{W}_p)|\,|\nabla\Pi_{K,p}(\boldsymbol{V}_p)| + |K_p|\left(|\boldsymbol{W}_K-\nabla\Pi_{K,p}(\boldsymbol{W}_p)|\right)\left(|\boldsymbol{V}_K-\nabla\Pi_{K,p}(\boldsymbol{V}_p)|\right) +$$

$$\left(\sum_{\zeta\in\mathcal{F}_{K,p}}|K_p|\,|\nabla\Pi_{K,p}(\boldsymbol{W}_p)|^2 + |K_p|h_{K,p}^{-2}\,|w_\zeta-w_K|^2\right)^{1/2}\left(\sum_{\zeta\in\mathcal{F}_{K,p}}|K_p|\,|\nabla\Pi_{K,p}(\boldsymbol{V}_p)|^2 + |K_p|h_{K,p}^{-2}\,|v_\zeta-v_K|^2\right)^{1/2},$$

from which the first result immediately follows using Cauchy-Schwarz inequality and the bound on $\nabla\Pi_{K,p}$. □

Being able to obtain this result is the reason why we have chosen to define operator $\boldsymbol{G}_{\mathcal{T}}$ through a global variational formulation. This is probably the major result of the present paper, as it provides existence and uniqueness of solution to the discrete problem (30) and as we will see that thanks to it the convergence theory is now very classical, up to some technicalities.

3 Convergence results

In the following, we will need to assume the following mesh regularity:

(MR) There exists $\theta_{\mathcal{M}} > 0$ and a matching simplicial submesh $\mathcal{SST}$ of $\mathcal{SM}$ such that for any $T \in \mathcal{SST}$, $\theta_{\mathcal{M}} h_T \leqslant r_T$ where r_T is the inradius of T, and for any $K \in \mathcal{T}$, any $p \in \mathcal{P}_K$ and any $T \in \mathcal{SST}$ such that $T \subset K_p$, $\theta_{\mathcal{M}} h_{K,p} \leqslant h_T$.

Assumption (MR) is slightly stronger than the usual mesh regularity assumption, in the sense that do not we require a matching simplicial submesh of the mesh $\mathcal{M}$ but of the submesh $\mathcal{SM}$: from this point of view, $\mathcal{SM}$ is the true mesh on which one should perform the numerical analysis. From [29], we know that for meshes satisfying (MR) $\theta_{\mathcal{F}}$ and θ_{Π} are bounded by a function of d and $\theta_{\mathcal{M}}$. The same holds for $\theta_{\mathcal{P}}$ for the examples of sets $\mathcal{P}$ of section 1.4.

Due do the importance of diffusion problems in applications and also because it is a kind of standard model problem for developing new numerical schemes, there exists a tremendous number of proofs and frameworks, more or less abstract, that provide convergence results for multiple point flux approximations. Without trying to be exhaustive, at the very least let us mention the classical two-point flux finite volume theory (see [39]), the theory of discontinuous Galerkin methods (see [29]), theory devoted to MPFA (see [8, 9]) and more general non-conforming methods (see [10, 30]), or the gradient discretization method (see [36]), the later being one of the widest and most recent abstract generalization of the previously mentioned approaches.

Because of the jumps allowed along internal subfaces $\zeta \in \mathcal{IF}$ and the additional boundary terms in the variational formulation, some of the elements of our method do not immediately coincide with those frameworks. Indeed, we need to show that our additional boundary terms do correspond to consistent terms that go to zero when h goes to zero, and that our discrete gradients are "limit conforming" (or equivalently "weakly consistent"). We do so thanks to the following two lemmas:

Lemma 3.1 (Consistency of boundary terms)**.** *For any $(\boldsymbol{W}, \boldsymbol{V}) \in X_0 \times X_0$, we have:*

$$\left| \sum_{K\in\mathcal{T}} \sum_{p\in\mathcal{P}_K} \sum_{\zeta\in\mathcal{IF}_{K,p}} |\zeta| \Lambda_K \boldsymbol{W}_K \cdot \boldsymbol{n}_{K,p,\zeta} v_{K,p,\zeta} \right| \leqslant \theta_{\Pi} \lambda^* |\boldsymbol{W}|_{1,X} \times$$

$$\left(\sum_{K\in\mathcal{T}} \sum_{p\in\mathcal{P}_K} \sum_{\zeta\in\mathcal{IF}_{K,p}} |K_p| h_{K,p}^{-2} |v_{K,p,\zeta} - v_K - \nabla\Pi_{K,p}(\boldsymbol{V}) \cdot (\boldsymbol{x}_\zeta - \boldsymbol{x}_K)|^2 + |K_p| |\boldsymbol{V}_K - \nabla\Pi_{K,p}(\boldsymbol{V})|^2 \right)^{1/2}.$$

Proof. As we have already seen in the proof of theorem 2.5, we have:

$$\begin{aligned}
&\sum_{K\in\mathcal{T}} \sum_{p\in\mathcal{P}_K} \sum_{\zeta\in\mathcal{IF}_{K,p}} |\zeta| \Lambda_K \boldsymbol{W}_K \cdot \boldsymbol{n}_{K,p,\zeta} v_{K,p,\zeta} \\
&= \sum_{K\in\mathcal{T}} \sum_{p\in\mathcal{P}_K} \sum_{\zeta\in\mathcal{IF}_{K,p}} |\zeta| \boldsymbol{W}_K \cdot \Lambda_K^T \boldsymbol{n}_{K,p,\zeta} \left(v_{K,p,\zeta} - v_K - \nabla\Pi_{K,p}(\boldsymbol{V}) \cdot (\boldsymbol{x}_\zeta - \boldsymbol{x}_K) \right) \\
&\quad - \sum_{K\in\mathcal{T}} \sum_{p\in\mathcal{P}_K} \sum_{\zeta\in\mathcal{IF}_{K,p}} |\zeta| \boldsymbol{W}_K \cdot \Lambda_K^T \boldsymbol{n}_{K,p,\zeta} \left(\boldsymbol{V}_K - \nabla\Pi_{K,p}(\boldsymbol{V}) \right) \cdot (\boldsymbol{x}_\zeta - \boldsymbol{x}_K),
\end{aligned}$$

and the result immediately follows by using Cauchy-Schwarz inequality. □

Lemma 3.2 (Limit conformity (or weak consistency) of the discrete gradients)**.** *Let $(\mathcal{M}_h)_{h\in\mathcal{H}}$ be a family of meshes indexed by $h\in\mathcal{H}$ where $\mathcal{H}$ is a bounded at most coutable subset of $\mathbb{R}^+$ such that $0\in\overline{\mathcal{H}}$ and there exists $\theta>0$ such that $max(\theta_{\mathcal{F}_h},\theta_{\mathcal{T}_h},\theta_{\Pi_h},\theta_{\mathcal{M}_h},\theta_{\mathcal{P}_h})\leqslant\theta$ for all $h\in\mathcal{H}$. Let us denote*

$$\Pi_{\mathcal{T}_h}(\boldsymbol{U}_h)|_K=u_K\quad\text{ and }\quad\hat{\nabla}_{\mathcal{T}_h}(\boldsymbol{U}_h)|_K=\sum_{p\in\mathcal{P}_K}\left(\frac{|K_p|}{|K|}\nabla\Pi_{K,p}(\boldsymbol{U}_h)-\sum_{\zeta\in\mathcal{IF}_{K,p}}\frac{|\zeta|}{|K|}u_{K,p,\zeta}\boldsymbol{n}_{K,p,\zeta}\right)\quad\forall\,K\in\mathcal{T}_h,$$

the piecewise constant function and weakly consistent gradient reconstructions. Then if $\boldsymbol{U}_h$ satisfies:

(ii) $\boldsymbol{U}_h\in X_{h,0}$ for all $h\in\mathcal{H}$,

(ii) $\Pi_{\mathcal{T}_h}(\boldsymbol{U}_h)\rightharpoonup u$ weakly in $L^2(\Omega)$ when $h\longrightarrow 0$,

(iii) there exists $C>0$ independent on h such that $|\boldsymbol{U}|_{1,X_h}\leqslant C$ for all $h\in\mathcal{H}$,

then $u\in H_0^1(\Omega)$, $\hat{\nabla}_{\mathcal{T}_h}(\boldsymbol{U}_h)\rightharpoonup\nabla u$ weakly in $L^2(\Omega)^d$ when $h\longrightarrow 0$.

Proof. Let us start by extending $\Pi_{\mathcal{T}_h}(\boldsymbol{U}_h)$ and $\hat{\nabla}_{\mathcal{T}_h}(\boldsymbol{U}_h)$ by 0 outside of Ω, and denote those extensions respectively $\widetilde{\Pi}_{\mathcal{T}_h}(\boldsymbol{U}_h)$ and $\widetilde{\nabla}_{\mathcal{T}_h}(\boldsymbol{U}_h)$. By virtue of lemma 2.1 and the fact that:

$$\sum_{\zeta\in\mathcal{IF}_{K,p}}|\zeta|u_{K,p,\zeta}\boldsymbol{n}_{K,p,\zeta}=\sum_{\zeta\in\mathcal{IF}_{K,p}}|\zeta|(u_{K,p,\zeta}-u_K)\boldsymbol{n}_{K,p,\zeta}$$

$$\leqslant\left(\sum_{\zeta\in\mathcal{IF}_{K,p}}|\zeta|h_{K,p}\right)^{1/2}\left(\sum_{\zeta\in\mathcal{IF}_{K,p}}|\zeta|h_{K,p}^{-1}|u_{K,p,\zeta}-u_K|^2\right)^{1/2}\leqslant\theta_\Pi\theta_{\mathcal{F}}^{1/2}|K_p|\left(\sum_{\zeta\in\mathcal{IF}_{K,p}}|K_p|h_{K,p}^{-2}|u_{K,p,\zeta}-u_K|^2\right)^{1/2},$$

we know that $||\widetilde{\nabla}_{\mathcal{T}_h}(\boldsymbol{U}_h)||_{L^2(\Omega)^d}$ is bounded and thus up to a subsequence there exists $\boldsymbol{G}\in L^2(\mathbb{R}^d)^d$ such that $\widetilde{\nabla}_{\mathcal{T}_h}(\boldsymbol{U}_h)\rightharpoonup\boldsymbol{G}$ weakly in $L^2(\mathbb{R}^d)^d$ when $h\to 0$ and that $\widetilde{\Pi}_{\mathcal{T}_h}(\boldsymbol{U}_h)\rightharpoonup\widetilde{u}$ weakly in $L^2(\mathbb{R}^d)$ when $h\to 0$, where $\widetilde{u}$ denotes the extension by zero of u outside Ω. Then notice that, for any $\Phi\in C_c^\infty(\mathbb{R}^d)^d$:

$$\int_{\mathbb{R}^d}\widetilde{\Pi}_{\mathcal{T}_h}(\boldsymbol{U}_h)\,div\,\Phi=\sum_{K\in\mathcal{T}_h}\sum_{p\in\mathcal{P}_K}\int_{K_p}u_K\,div\,\Phi,$$

which leads to:

$$\int_{\mathbb{R}^d}\widetilde{\Pi}_{\mathcal{T}_h}(\boldsymbol{U}_h)\,div\,\Phi=\sum_{K\in\mathcal{T}_h}\sum_{p\in\mathcal{P}_K}\sum_{\zeta\in\mathcal{F}_{K,p}}|\zeta|u_K\Phi_\zeta\cdot\boldsymbol{n}_{K,p,\zeta}\quad\text{ with }\quad\Phi_\zeta=\frac{1}{|\zeta|}\int_\zeta\Phi.$$

Then, recall that for any $p\in\mathcal{P}_K$ and any $\zeta\in\mathcal{SF}_{K,p}$ we have denoted $u_{K,p,\zeta}=u_\zeta$ with $\Phi_\zeta=0$ for any $\zeta\in\mathcal{SF}_{ext}$ thus

$$\sum_{K\in\mathcal{T}_h}\sum_{p\in\mathcal{P}_K}\sum_{\zeta\in\mathcal{SF}_{K,p}}|\zeta|u_{K,p,\zeta}\Phi_\zeta\cdot\boldsymbol{n}_{K,p,\zeta}=\sum_{\zeta\in\mathcal{SF}_{int}}|\zeta|u_\zeta\Phi_\zeta\cdot\left(\sum_{K\in\mathcal{T}_\zeta}\sum_{p\in\mathcal{P}_K}\sum_{|\ \zeta\in\mathcal{SF}_{K,p}}\boldsymbol{n}_{K,p,\zeta}\right)=0.$$

Denoting $\Phi_K=\frac{1}{|K|}\int_K\Phi$, this leads to:

$$\int_{\mathbb{R}^d}\widetilde{\Pi}_{\mathcal{T}_h}(\boldsymbol{U}_h)\,div\,\Phi=$$

$$\sum_{K\in\mathcal{T}_h}\sum_{p\in\mathcal{P}_K}\sum_{\zeta\in\mathcal{F}_{K,p}}|\zeta|(u_K-u_{K,p,\zeta})\Phi_\zeta\cdot\boldsymbol{n}_{K,p,\zeta}+\sum_{K\in\mathcal{T}_h}\sum_{p\in\mathcal{P}_K}\sum_{\zeta\in\mathcal{IF}_{K,p}}|\zeta|u_{K,p,\zeta}\Phi_\zeta\cdot\boldsymbol{n}_{K,p,\zeta}$$

$$= \sum_{K\in\mathcal{T}_h}\sum_{p\in\mathcal{P}_K}\sum_{\zeta\in\mathcal{F}_{K,p}} |\zeta|(u_K - u_{K,p,\zeta})\Phi_K\cdot\boldsymbol{n}_{K,p,\zeta}$$

$$+ \sum_{K\in\mathcal{T}_h}\sum_{p\in\mathcal{P}_K}\sum_{\zeta\in\mathcal{F}_{K,p}} |\zeta|(u_K - u_{K,p,\zeta})(\Phi_\zeta - \Phi_K)\cdot\boldsymbol{n}_{K,p,\zeta} + \sum_{K\in\mathcal{T}_h}\sum_{p\in\mathcal{P}_K}\sum_{\zeta\in\mathcal{IF}_{K,p}} |\zeta|u_{K,p,\zeta}\Phi_\zeta\cdot\boldsymbol{n}_{K,p,\zeta}$$

$$= -\sum_{K\in\mathcal{T}_h}\sum_{p\in\mathcal{P}_K} |K_p|\nabla_{K,p}(\boldsymbol{U}_h)\cdot\Phi_K + \sum_{K\in\mathcal{T}_h}\sum_{p\in\mathcal{P}_K}\sum_{\zeta\in\mathcal{IF}_{K,p}} |\zeta|u_{K,p,\zeta}\Phi_K\cdot\boldsymbol{n}_{K,p,\zeta}$$

$$\sum_{K\in\mathcal{T}_h}\sum_{p\in\mathcal{P}_K}\sum_{\zeta\in\mathcal{F}_{K,p}} |\zeta|(u_K - u_{K,p,\zeta})(\Phi_\zeta - \Phi_K)\cdot\boldsymbol{n}_{K,p,\zeta} + \sum_{K\in\mathcal{T}_h}\sum_{p\in\mathcal{P}_K}\sum_{\zeta\in\mathcal{IF}_{K,p}} |\zeta|(u_{K,p,\zeta} - u_K)(\Phi_\zeta - \Phi_K)\cdot\boldsymbol{n}_{K,p,\zeta}$$

$$= -\sum_{K\in\mathcal{T}_h}\int_K \hat{\nabla}_{\mathcal{T}_h}(\boldsymbol{U}_h)\cdot\Phi_K + T_1 + T_2,$$

with obvious notations and as $\sum_{K\in\mathcal{T}_h}\sum_{p\in\mathcal{P}_K}\sum_{\zeta\in\mathcal{IF}_{K,p}} |\zeta|u_K(\Phi_\zeta - \Phi_K)\cdot\boldsymbol{n}_{K,p,\zeta} = 0$. Using the fact that $|\Phi_\zeta - \Phi_K| \leqslant C_\Phi h_K$ for some $C_\Phi > 0$ independent on h, the bound on the remaining terms T_1 and T_2 are classical, as we have using Cauchy-Schwarz inequality:

$$|T_1| \leqslant C_\Phi h \left(\sum_{K\in\mathcal{T}_h}\sum_{p\in\mathcal{P}_K}\sum_{\zeta\in\mathcal{F}_{K,p}} |\zeta|h_{K,p}\right)^{1/2}\left(\sum_{K\in\mathcal{T}_h}\sum_{p\in\mathcal{P}_K}\sum_{\zeta\in\mathcal{F}_{K,p}} |\zeta|h_{K,p}^{-1}|u_K - u_{K,p,\zeta}|^2\right)^{1/2},$$

and

$$|T_2| \leqslant C_\Phi h \left(\sum_{K\in\mathcal{T}_h}\sum_{p\in\mathcal{P}_K}\sum_{\zeta\in\mathcal{IF}_{K,p}} |\zeta|h_{K,p}\right)^{1/2}\left(\sum_{K\in\mathcal{T}_h}\sum_{p\in\mathcal{P}_K}\sum_{\zeta\in\mathcal{IF}_{K,p}} |\zeta|h_{K,p}^{-1}|u_K - u_{K,p,\zeta}|^2\right)^{1/2},$$

and thus $|T_i| \leqslant C_\Phi\theta_{\mathcal{F}_h}^{1/2}\theta_{\mathcal{P}_h}^{1/2}\theta_{\Pi_h}|\Omega|^{1/2}|\boldsymbol{U}|_{1,X_h}$ for $i\in\{1,2\}$, which directly leads to $\hat{\nabla}_{\mathcal{T}_h}(\boldsymbol{U}_h) \rightharpoonup \nabla\widetilde{u}$ weakly in $L^2(\mathbb{R})^d$ when $h\to 0$. Thus $\boldsymbol{G} = \nabla\widetilde{u}$, which implies $\widetilde{u}\in H^1(\mathbb{R}^d)$ and consequently $u\in H_0^1(\Omega)$. □

The remaining necessary properties to establish convergence are the stability of the method, which we already have, as well as the strong consistency of the gradient and the stabilization term. As we have used the hybrid gradient in our local variational problems, establishing the consistency of $\nabla\Pi_{K,p}$ is completely classical, which in turns immediately imply the strong consistency of the stabilization, boundary terms and of the weakly consistent gradient $\hat{\nabla}_{\mathcal{T}}$, using of course for v regular enough $\boldsymbol{V}_K = \nabla v(\boldsymbol{x}_K)$ and $v_{K,p,\zeta} = v(\boldsymbol{x}_\zeta)$ for the additional degrees of freedom of our enriched MPFA, thanks to either lemma 3.1 or

$$\sum_{p\in\mathcal{P}_K \mid \zeta\in\mathcal{IF}_{K,p}} \frac{|\zeta|}{|K|}v(\boldsymbol{x}_\zeta)\boldsymbol{n}_{K,p,\zeta} = 0.$$

Combining those classical results with the fact that we have established the desired properties for our unusual terms, using one's favorite option among the many available frameworks (and in particular such as [10] or [30] for the non-symmetric case) it is now a classical matter to obtain the following convergence results for our stable MPFA (SMPFA) method:

Proposition 3.3. *Let $d = 2$ or 3, and assume that the meshes satisfy (MR). Then, we have:*

(i) Let $(\mathcal{M}_h)_{h\in\mathcal{H}}$ be a family of meshes indexed by $h\in\mathcal{H}$ where $\mathcal{H}$ is a bounded at most countable subset of $\mathbb{R}^+$ such that $0\in\overline{\mathcal{H}}$ and there exists $\theta > 0$ such that $\theta > 0$ such that $max(\theta_{\mathcal{F}_h},\theta_{\mathcal{T}_h},\theta_{\Pi_h},\theta_{\mathcal{M}_h},\theta_{\mathcal{P}_h}) \leqslant \theta$ for all $h\in\mathcal{H}$. Then if $\boldsymbol{U}_h$ denotes the solution of the multiple point flux approximation associated to mesh $\mathcal{M}_h$, we have when $h\longrightarrow 0$

$$||\Pi_{\mathcal{T}_h}(\boldsymbol{U}_h)\overline{u}||_{L^2(\Omega)} \longrightarrow 0 \quad \textit{and} \quad ||\nabla_{\mathcal{T}_h}(\boldsymbol{U}_h) - \nabla\overline{u}||_{L^2(\Omega)^d} \longrightarrow 0 \quad \textit{and} \quad ||\boldsymbol{G}_{\mathcal{T}_h}(\boldsymbol{U}_h) - \nabla\overline{u}||_{L^2(\Omega)^d} \longrightarrow 0,$$

where the piecewise constant function and gradient reconstructions are given for all $K \in \mathcal{T}_h$ by:

$$\Pi_{\mathcal{T}_h}(\boldsymbol{U}_h)|_K = u_K \quad \textit{and} \quad \nabla_{\mathcal{T}_h}(\boldsymbol{U}_h)|_K = \sum_{p\in\mathcal{P}_K} \frac{|K_\zeta|}{|K|}\nabla\Pi_{K,\zeta}(\boldsymbol{U}_h) \quad \textit{and} \quad G_{\mathcal{T}_h}(\boldsymbol{U}_h)|_K = \boldsymbol{G}_K(\boldsymbol{U}_h).$$

(ii) If $\Lambda \in W^{1,\infty}(\Omega)$ and $\overline{u} \in H_0^1(\Omega) \cap H^2(\Omega)$, then there exists $C_u > 0$ depending on u, Ω, λ_*, λ^*, $\theta_{\mathcal{F}}$, $\theta_{\mathcal{T}}$, θ_Π, $\theta_{\mathcal{P}}$ but independent on h such that:

$$||\Pi_{\mathcal{T}}(\boldsymbol{U}) - \overline{u}||_{L^2(\Omega)} \leqslant C_u h \quad \textit{and} \quad ||\nabla_{\mathcal{T}}(\boldsymbol{U}) - \nabla\overline{u}||_{L^2(\Omega)^d} \leqslant C_u h \quad \textit{and} \quad ||G_{\mathcal{T}}(\boldsymbol{U}) - \nabla\overline{u}||_{L^2(\Omega)^d} \leqslant C_u h.$$

Notice that the convergence and error estimates for $\boldsymbol{G}_{\mathcal{T}}(\boldsymbol{U})$ are in fact obtained a posteriori thanks to the fact

$$\sum_{K\in\mathcal{T}}\sum_{p\in\mathcal{P}_K} \lambda^1_{K,p}|\boldsymbol{V}_K - \nabla\Pi_{K,\zeta}(\boldsymbol{V})|^2 \leqslant a_h(\boldsymbol{V},\boldsymbol{V}),$$

and proceeding in the same way than for establishing the strong convergence of $\nabla_{\mathcal{T}}(\boldsymbol{U})$. We thus know that our new MPFA methods will have the desired convergence behavior. Let us also mention that up to some additional (mainly technical) hypothesis, it is feasible to obtain superconvergence of the L^2 reconstruction for the symmetric version $\mu = 1$, i.e. $||\Pi_{\mathcal{T}_h}(\boldsymbol{U}_h) - \overline{u}||_{L^2(\Omega)} \leqslant C_u h^2$ using the classical Aubin-Nitsche's duality argument (see [37, 36]). As the global formulation for the non-symmetric version ($\mu = 0$) is formally very close to the IIP discontinuous Galerkin method, we expect that super-convergence can be lost for the non-symmetric version in specific cases (see [49]).

4 Numerical experiments

In this section, we test our stable MPFA method (SMPFA) on the classical set of test cases used for instance in [20]. We consider six SMPFA schemes: the SMPFA schemes based on faces in symmetric (SMPFA-FS) and non-symmetric (SMPFA-FN) versions, the SMPFA schemes based on subfaces in symmetric (SMPFA-SS) and non-symmetric versions (SMPFA-SN), and the SMPFA schemes using the O-shaped domain in symmetric (SMPFA-OS) and non-symmetric (SMPFA-ON) versions. Notice that in dimension two, in practice we use faces as subfaces ($\mathcal{F} = \mathcal{SF}$) and the schemes based on subfaces and faces are identical, thus we will only display results for (SMPFA-F). All the SMPFA schemes are used with $\omega = 0.5$, $\gamma_0 = 0.9$ and $\gamma_1 = 0.01$. We compare the SMPFA schemes to other unconditionally stable finite volume approaches: the hybrid finite volume scheme ([40, 41]), the original VAG scheme of [42] as well as the naturally stable variant VAGRT based on a tetrahedral subdivision of cells of [47], and the conservative first order VEM called virtual volumes (VVM) of [20]. Finally, we also consider the classical conditionally stable MPFA-O method ([1]). For simplicity, the L^2 convergence results that will be plotted correspond to $\sqrt{\sum_{K\in\mathcal{T}}|K|(u(\boldsymbol{x}_K) - u_K)^2}$ where u is the exact solution. Apart from the MPFAO scheme, all other finite volume methods used here require additional unknowns, corresponding to of course our additional cell unknowns for our SMPFA schemes, mesh faces for the hybrid scheme, and to mesh vertices for all the other ones. Thus, a fair comparison cannot rely only on classical convergence curves against h, as the different methods use different sets of unknowns. We consequently also display convergence curves in terms of the total number of unknowns.

4.1 Numerical results in dimension 2

We consider the domain $\Omega =]0,1[\times]0,1[$ which is subdivided into four areas, denoted D_i, $i = 1..4$, and we use a sequence of meshes fitting this partition (see figure 5). On this domain, we consider the three tests cases of [7] and [46], that allow to study the behavior of the method in presence of strong heterogeneity and

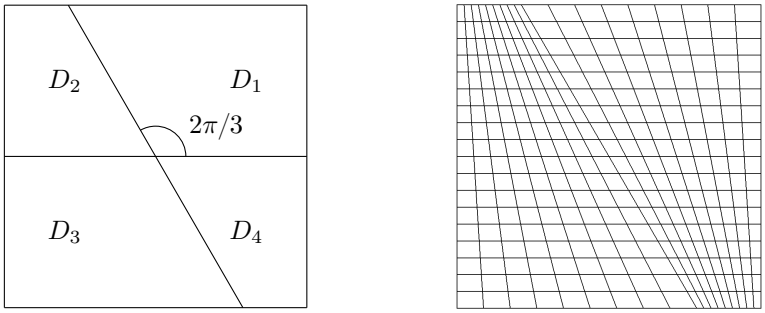

Figure 5: Domain subdivision and example of mesh

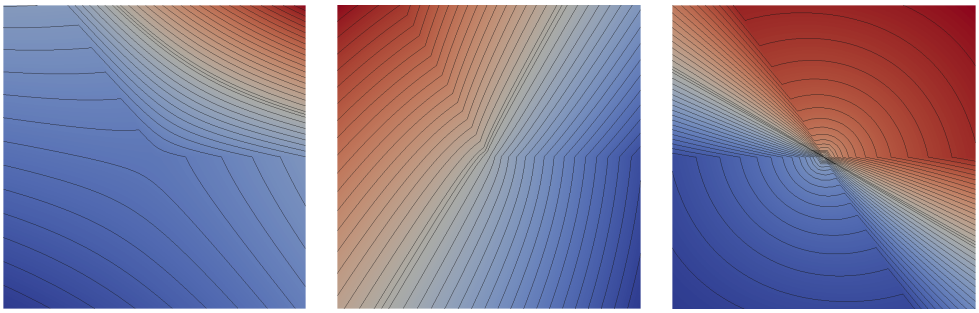

Figure 6: Isolines of solutions for *ConvTest1*, *ConvTest2* and *ConvTest3*

for low regularity solutions. The first test case (named *ConvTest1*, see figure 6) is such that $\Lambda_{|_{D_1}} = \lambda_1 Id$ and $\Lambda_{|_{\Omega\setminus D_1}} = \lambda_2 Id$. A solution of $-div(\Lambda\nabla u) = 0$ is then given by :

$$u = \left| \begin{array}{ll} r^\alpha \cos(\alpha(\theta - \pi/3)) & \text{for } \theta \in [0, 2\pi/3], \\ \beta r^\alpha \cos(\alpha(4\pi/3 - \theta)) & \text{for } \theta \in [2\pi/3, 2\pi], \end{array} \right. \tag{34}$$

with $\alpha = (3/\pi)\arctan\sqrt{1 + 2/\kappa}$ and $\beta = \cos(\alpha\pi/3)/\cos(2\alpha\pi/3)$, and $\kappa = \lambda_1/\lambda_2 = 0.1$. For the same tensor, the second test case (named *ConvTest2*, see figure 6), is given by

$$u = \left| \begin{array}{ll} r^\alpha \sin(\alpha(\theta - \pi/3)) & \text{for } \theta \in [0, 2\pi/3], \\ \beta r^\alpha \sin(\alpha(4\pi/3 - \theta)) & \text{for } \theta \in [2\pi/3, 2\pi], \end{array} \right. \tag{35}$$

with $\alpha = (3/\pi)\arctan\sqrt{1 + 2\kappa}$ and $\beta = 1/(2\cos(\alpha\pi/3))$, and $\kappa = \lambda_1/\lambda_2$. Finally, for $\Lambda_{|_{D_1}} = \Lambda_{|_{D_3}} = \lambda_1 Id$ and $\Lambda_{|_{D_2}} = \Lambda_{|_{D_4}} = \lambda_2 Id$, the third test case (named *ConvTest3*, see figure 6) is given by $u(r, \theta) = -u(r, \theta - \pi)$ and

$$u = \left| \begin{array}{ll} r^\alpha \cos(\alpha(\theta - \pi/3)) & \text{for } \theta \in [0, 2\pi/3], \\ \beta r^\alpha \sin(\alpha(5\pi/6 - \theta)) & \text{for } \theta \in [2\pi/3, \pi], \end{array} \right. \tag{36}$$

with $\alpha = (6/\pi)\arctan\left(1/\sqrt{1 + 2\kappa}\right)$ and $\beta = \cos(\alpha\pi/3)/\sin(\alpha\pi/6)$, and $\kappa = \lambda_1/\lambda_2 = 30$. The solutions of *convTest1*, *ConvTest2* and *ConvTest3* have the respective approximate regularities $H^{2.29}$, $H^{1.79}$ and $H^{1.24}$, as

$\alpha \approx 1.29$ for *ConvTest1*, $\alpha \approx 0.79$ for *ConvTest2* and $\alpha \approx 0.24$ for *ConvTest3*. From the results displayed in figures 10, 11 and 12, we deduce the approximate convergence orders of table 1. Apart for the SMPFA-ON scheme, all are in agreement with the optimal order of $min(2, 2\alpha)$ which is 2 for the *ConvTest1*, 1.58 for *ConvTest2* and 0.48 for *ConvTest3*. The SMPFA-ON scheme does not superconverge for *ConvTest1* and *ConvTest2* , which is probably the effect of the non-symmetry. Also notice that its symmetric version SMPFA-OS outperforms all other schemes on the low regular *ConvTest3*.

Table 1: Approximate orders of convergence for *ConvTest1*, *ConvTest2* and *ConvTest3*

	ConvTest1	*ConvTest2*	*ConvTest3*
SMPFA-FS	1.99	1.72	0.53
SMPFA-FN	2.02	1.51	0.47
SMPFA-OS	1.75	1.60	0.86
SMPFA-ON	1.05	0.88	0.45
MPFAO	2.06	1.56	0.45
Hybrid	1.97	1.55	0.39
VAG	1.98	1.52	0.53
VAGRT	2.07	1.53	0.54
VVM	1.97	1.59	0.50

Then, to assess the behavior of the method in presence of anisotropy and on distorted mesh, still on $\Omega =]0,1[\times]0,1[$, we consider

$$u(x,y) = sin(\pi x)sin(\pi y) \qquad \Lambda = \begin{pmatrix} 1 & 0 \\ 0 & \epsilon \end{pmatrix}, \tag{37}$$

with $\epsilon = 10^{-2}$, which will be named *ConvTest4*. We consider five types of mesh sequences. The first one is a sequence of Delaunay meshes (*2dDelaunay*), while the second one (*2dDualDelaunay*) is obtained by considering the dual meshes of the first sequence. The third one (*2dVoronoi*) is the sequence of Voronoï meshes associated to the same sequence of Delaunay meshes. The fourth sequence (*2dKershawBox*) is a sequence of Kershaw meshes of the unit square, and finally the fifth one (*2dCheckerBoardBox*) is a sequence of checkerboard meshes of the unit square. These two sequences have only quadrangular cells which are distorted for the sequence *2dKershawBox*, while the sequence *2dCheckerBoardBox* allows to test the behavior of the method in presence of non conformities.

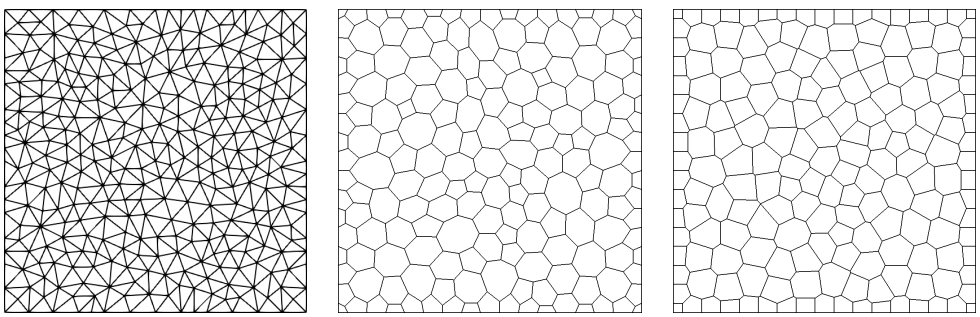

Figure 7: Example of meshes for the *2dDelaunay*, *2dDualDelaunay* and *2dVoronoi* mesh sequences

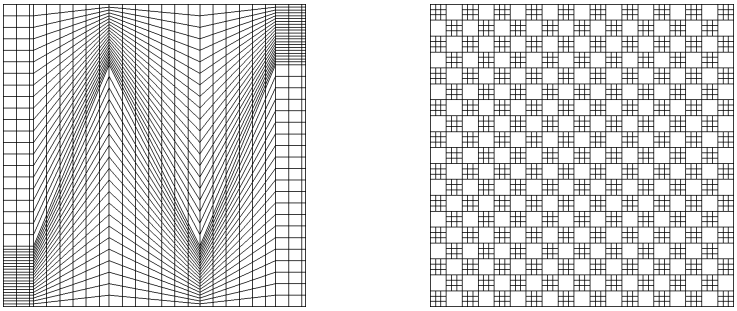

Figure 8: Example of meshes for the *2dKershawBox* and *2dCheckerBoardBox* mesh sequences

Table 2: Approximate orders of convergence for *ConvTest4*

	2dDelaunay	*2dDualDelaunay*	*2dVoronoi*	*2dKershawBox*	*2dCheckerBoardBox*
SMPFA-FS	1.93	2.13	2.04	1.92	2.06
SMPFA-FN	1.93	2.10	2.04	1.91	2.06
SMPFA-OS	2.06	2.09	2.00	1.35	2.04
SMPFA-ON	2.03	2.03	1.97	1.65	2.04
MPFAO	-	-	1.84	1.94	2.04
Hybrid	1.93	2.17	2.02	1.91	2.33
VAG	2.02	2.19	2.04	1.52	1.99
VAGRT	2.02	2.08	1.98	1.66	1.94
VVM	2.03	2.24	2.14	1.79	2.01

The convergence curves are displayed on the five figures 13-14-15-16-17, each one corresponding to one of the mesh sequences, while the approximate convergence orders are given in table 4.1. Notice that the MPFAO scheme exhibits instabilities for the *2dDelaunay* and *2dDualDelaunay* mesh sequences. All the other schemes converge on all the mesh sequences with the expected convergence order. Nevertheless notice that on the *2dDelaunay* mesh sequence, the error constant of the Hybrid scheme is quite high, most probably because of some non-alignment of the gradients on this anisotropic test case for this very specific mesh sequence: indeed, on simplicies the classical stabilization terms cannot compensate for those alignments problems. Naturally the same holds for the SMPFA-FS and SMPFA-FN for which the subproblems will share the same deficiencies. Numerical experiments reveals that adding extra stabilization terms (under the form $|K_p|h_{K,p}^2 \nabla_{K,p}(\boldsymbol{U})\nabla_{K,p}(\boldsymbol{V})$) improves the convergence of both the Hybrid and SMPFA-F schemes on this mesh sequence. For the *2dKershawBox* mesh sequence that do not really satisfy (MR), we can see some effect of the mesh irregularity: the convergence is slower for all schemes, and in particular for the SMPFA-OS, SMPFA-ON, VAG and VAGRT schemes. For the SMPFA-O schemes, the reason is most likely the fact that the subcells K_p become highly distorted, thus θ_Π grows which increases the contribution to the error of the stabilization terms. On this mesh sequence, the SMPFA-F versions are clearly a better option than the SMPFA-O, contrary to what happened for the *2dDelaunay* mesh sequence. Concerning the three other mesh sequences, all the stable finite volume schemes perform comparably, the "best" scheme not being the same for every mesh sequence.

Figures 13-14-15-16-17 also reveals the evolution of the L^2 error with the total number of unknowns. First, it reminds that apart for the MPFAO scheme, the number of unknowns for a given scheme is highly dependent

on the geometry of the cells: the Hybrid scheme for instance has much less unknowns on simplices (where it is also less good) than on Voronoï cells. The main point is to notice that the more complex the cells, the better the number of unknowns of the SMPFA scheme will compare with other approaches. Moreover in general for a given number of unknowns the L^2 error of the SMPFA schemes are competitive when compared with the other finite volume schemes. Nevertheless, we must mention that for the VAG, VAGRT, VVM and Hybrid schemes, the cell unknowns can be eliminated from the linear system through static condensation. We have not at this stage worked on a way to reduce the size of the final linear systems for the SMPFA schemes, hybridization techniques (see [12, 21]) probably being the right approach.

Finally, let us mention that when the non-symmetric versions of the SMPFA scheme superconverge, they always outperform their symmetric counterpart, as should be expected: indeed, the symmetric version adds an extra stabilization term that increases the overall approximation error.

4.2 Numerical results in dimension 3

We now perform a few experiments in dimension 3. To assess the behavior of the method in presence of anisotropy and on distorted mesh, we consider

$$u(x,y) = sin(\pi x)sin(\pi y)sin(\pi z) \qquad \Lambda = \begin{pmatrix} \epsilon & 0 & 0 \\ 0 & \epsilon & 0 \\ 0 & 0 & 1.0 \end{pmatrix}, \tag{38}$$

with $\epsilon = 10^{-2}$. We test this solution on a Cartesian mesh sequence of the unit cube (named *3dBox*), a checkerboard mesh sequence (*3dCheckerBoardBox*), a randomly perturbed cartesian mesh *3dRandomBox*, as well as the distorted mesh sequence *3dSweep* displayed on figure 4.2. Meshes of these last sequence are obtained by mapping a polygonal mesh of the unit square in the xy plane to a non planar surface. For the last two sequences, the planar subfaces are obtained by splitting the non planar into triangles based on the face's barycenter.

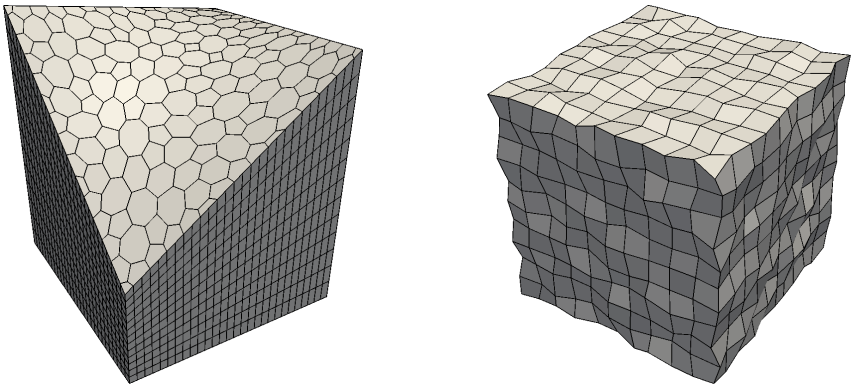

Figure 9: Example of meshes for the *3dSweep* and *3dBoxRandom* mesh sequences

The results are presented on figures 18-19-20-21, with the corresponding approximate convergence orders in table 3. The observations are roughly speaking the same than in dimension 2. The main point is the fact that the face and subface based SMPFA schemes are no longer the same in dimension 3: on our examples, because the subface based local domains D_ζ are more distorted for the *3dSweep* and *3dRandomBox* sequences that their face based counterparts D_σ, we see that the face based versions outperform the subface based ones.

Table 3: Approximate orders of convergence for *ConvTest5*

	3dBox	*3dCheckerBoardBox*	*3dSweep*	*3dRandomBox*
SMPFA-FS	2.00	2.10	2.33	2.18
SMPFA-FN	1.99	2.04	2.31	2.25
SMPFA-SS	2.00	2.10	1.64	1.86
SMPFA-SN	1.99	2.04	1.96	2.11
SMPFA-OS	1.86	1.97	2.00	2.34
SMPFA-ON	1.95	1.99	2.22	2.20
MPFAO	1.96	1.76	-	-
Hybrid	2.00	2.29	2.47	1.63
VAG	1.90	1.95	2.05	2.25
VAGRT	2.00	1.59	2.08	2.48
VVM	1.94	1.93	2.25	2.50

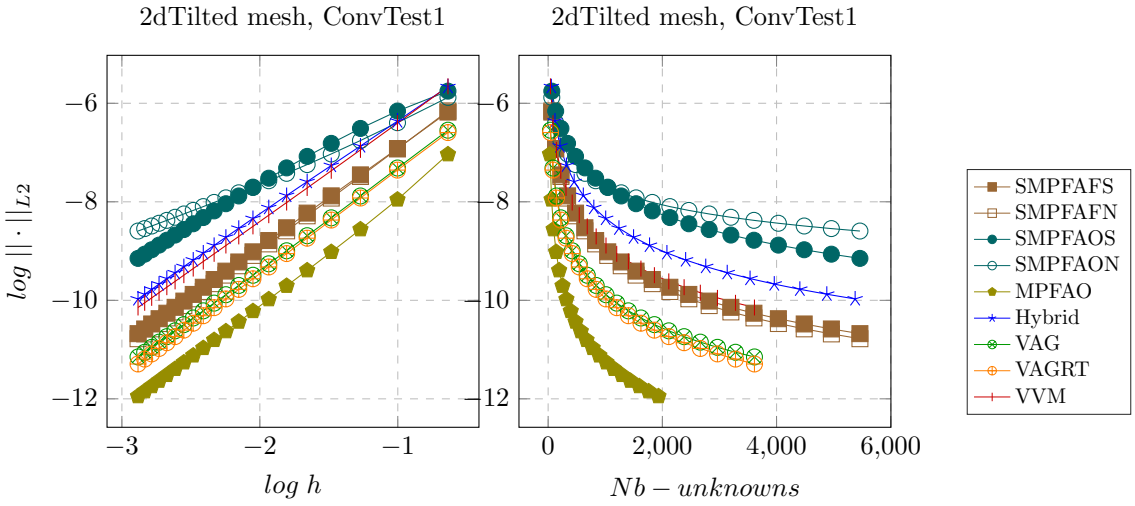

Figure 10: Convergence curves for *ConvTest1*

Conclusion

We have presented a family of enriched multiple point flux approximation leading to fully cell-centered finite volume schemes using additional cell unknowns. Both symmetric and non-symmetric versions were introduced, and the unconditional stability of the methods was established for general meshes. The convergence theory follows from established frameworks, and numerical results were exhibited to emphasize the good behavior of the approach on challenging tests cases. On going works concern the extension of the method to linear elasticity as well as increasing the stability of the face-based version on simplicies. Future work will concern the application of the SMPFA to porous media flow.

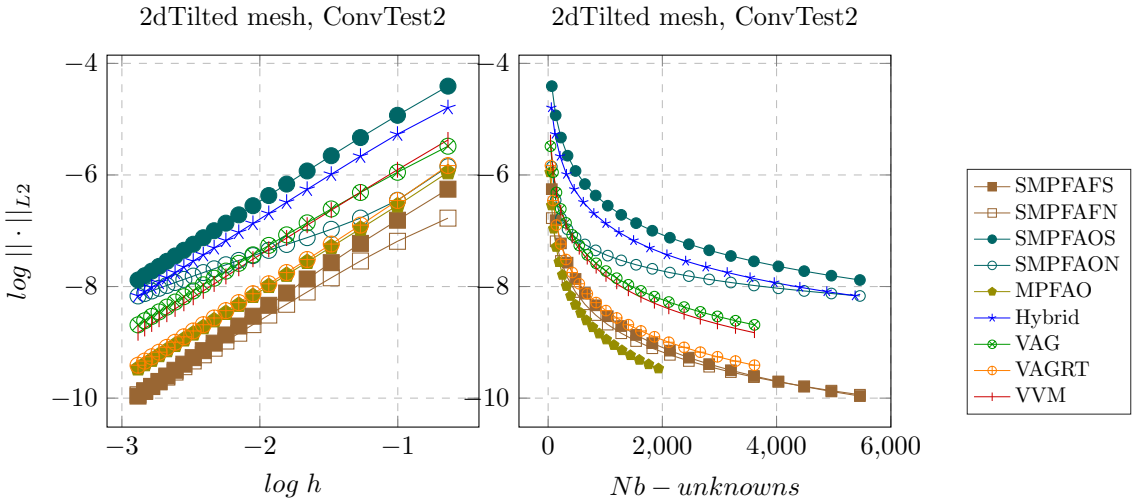

Figure 11: Convergence curves for *ConvTest2*

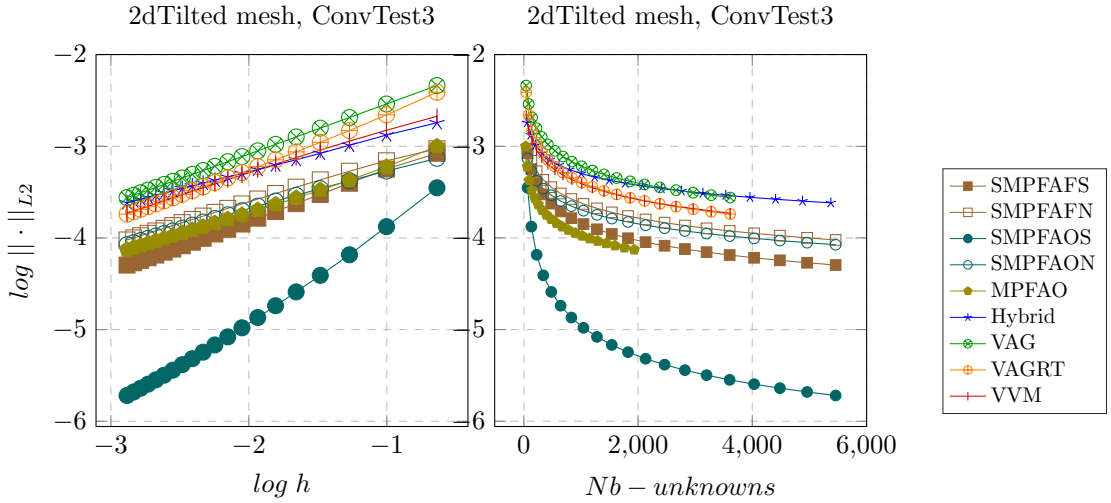

Figure 12: Convergence curves for *ConvTest3*

REFERENCES

[1] I. Aavatsmark, T. Barkve, O. Boe, and T. Mannseth. Discretization on non-orthogonal, curvilinear grids for multi-phase flow. *Proceedings of the fourth European Conference on the Mathematics of Oil Recovery, Norway*, 1994.

[2] I. Aavatsmark, T. Barkve, O. Boe, and T. Mannseth. Discretization on non-orthogonal, quadrilateral grids for inhomogeneous, anisotropic media. *J. Comput. Phys., Vol. 127(1), pp. 2-14*, 1996.

[3] I. Aavatsmark, T. Barkve, O. Boe, and T. Mannseth. Discretization on unstructured grids for inhomogeneous, anisotropic media part i: Derivation of the methods. *SIAM Journal on Sc. Comp., Vol. 19, pp. 1700-1716*, 1998.

[4] I. Aavatsmark, T. Barkve, O. Boe, and T. Mannseth. Discretization on unstructured grids for inhomogeneous,

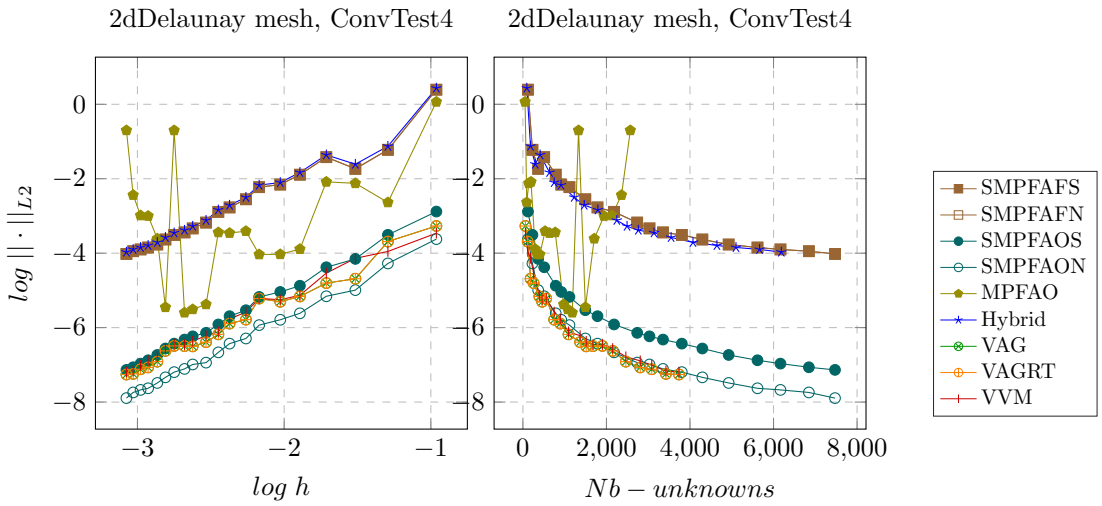

Figure 13: Convergence curves for *Sinusoidal2D* for the *2dDelaunay* mesh sequence

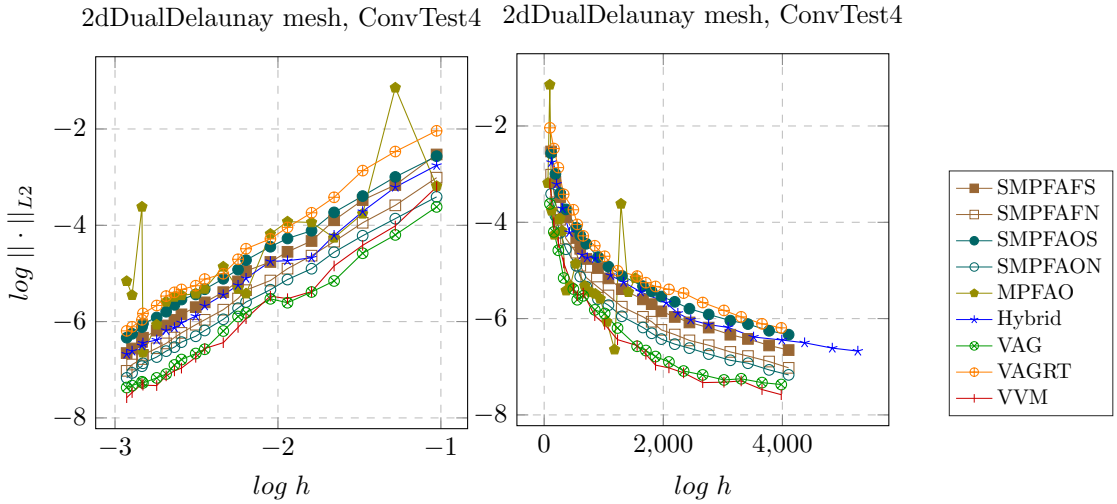

Figure 14: Convergence curves for *Sinusoidal2D* for the *2dDualDelaunay* mesh sequence

anisotropic media. part ii: Discussion and numerical results. *SIAM Journal on Sc. Comp., Vol. 19, pp.1717-1736*, 1998.

[5] I. Aavatsmark and G. T. Eigestad. Numerical convergence of the mpfa o-method and u-method for general quadrilateral grids. *Int. J. Numer. Meth. Fluids, Vol. 51, pp. 939-961*, 2005.

[6] I. Aavatsmark, G. T. Eigestad, B. O. Heimsund, B. T. Mallison, J. M. Nordbotten, and E. Oian. A new finite-volume approach to efficient discretization on challenging grids. *SPE Journal, Vol. 15(3), pp. 658-669*, 2010.

[7] I. Aavatsmark, G. T. Eigestad, B. T. Mallison, and J. M. Nordbotten. A compact multipoint flux approximation method with improved robustness. *Numerical Methods For Partial Differential Equations, Vol. 4, pp. 1329-1360*, 2008.

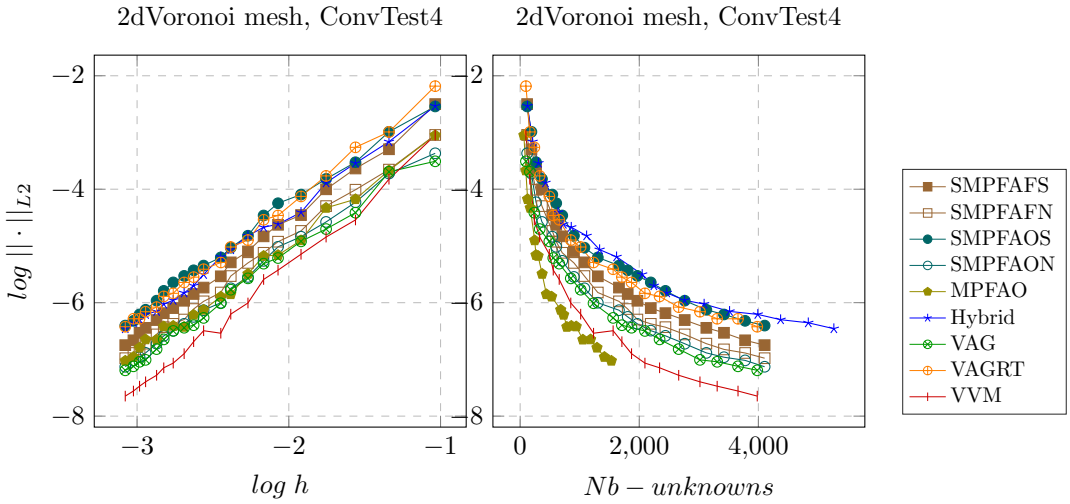

Figure 15: Convergence curves for *Sinusoidal2D* for the *2dVoronoi* mesh sequence

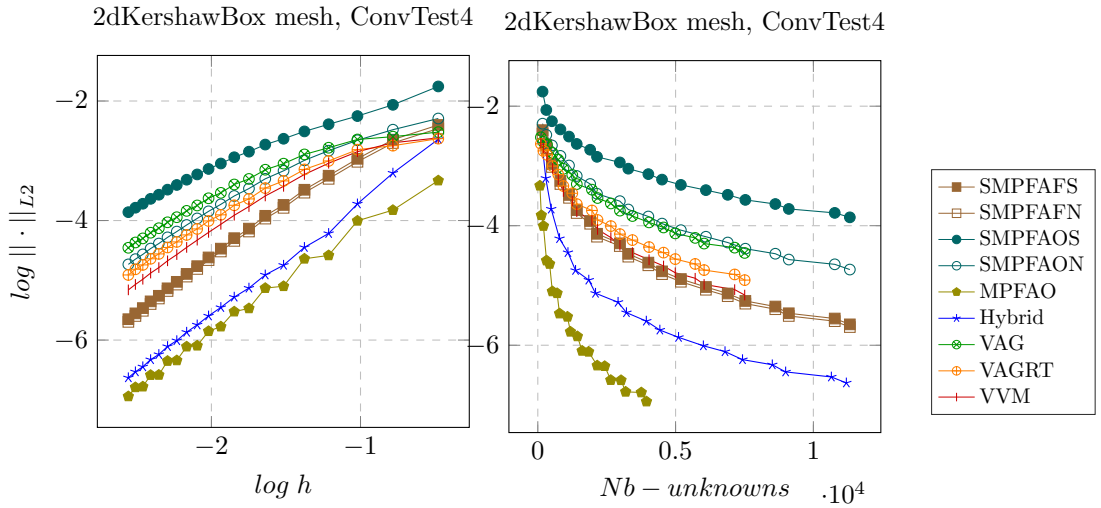

Figure 16: Convergence curves for *Sinusoidal2D* for the *2dKershawBox* mesh sequence

[8] L. Agélas and R. Masson. Convergence of finite volume mpfa o type schemes for heterogeenous anisotropic diffusion problems on general meshes. *C.R. Acad. Paris, Ser. I 346*, 2008.

[9] L. Agélas, D.A. Di Pietro, and J. Droniou. The g method for heterogeneous anisotropic diffusion on general meshes. *ESAIM Math. Model. Numer. Anal., 11 pp 597-625*, 2010.

[10] L. Agélas, D.A. Di Pietro, R. Eymard, and R. Masson. An abstract analysis framework for nonconforming approximations of anistropic heterogeneous diffusion problems. *IJFV International Journal On Finite Volumes, Vol. 7(1)*, 2010.

[11] L. Agélas, D.A. Di Pietro, and R. Masson. A symmetric and coercive finite volume scheme for multiphase porous media flow problems with applications in the oil industry. *In R. Eymard ans J.-M. Hérard, Finite volume for Complex Applications V, pp. 35-51, Wiley*, 2008.

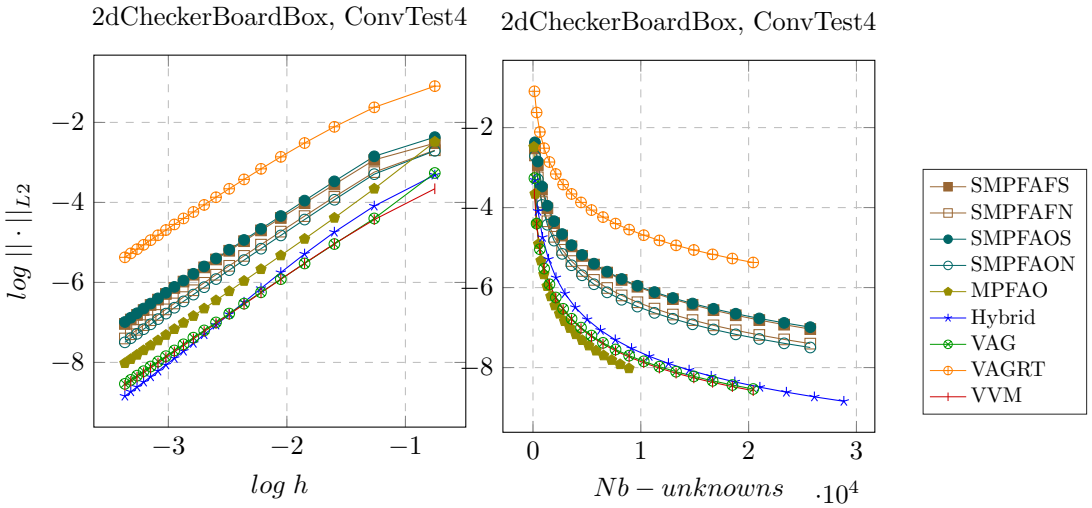

Figure 17: Convergence curves for *Sinusoidal2D* for the *2dCheckerBoardBox* mesh sequence

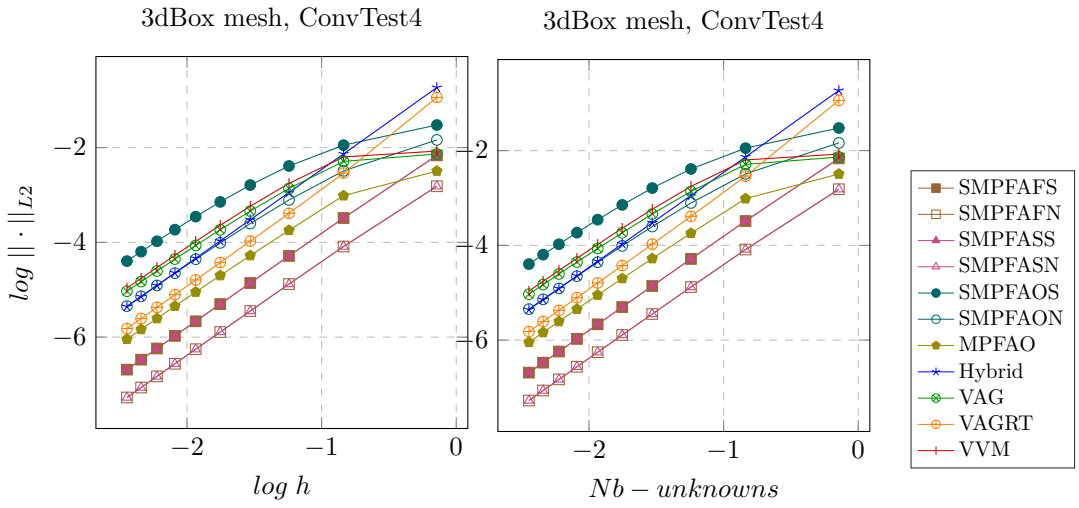

Figure 18: Convergence curves for *Sinusoidal3D* for the *3dBox* mesh sequence

[12] D. N. Arnold and F. Brezzi. Mixed and nonconforming finite element methods: implementation, post-processing and error estimates. *RAIRO Model. Math. Anal. Num., Vol. 19(4), PP.7-32*, 1985.

[13] D. N. Arnold, F. Brezzi, B. Cockburn, and L.D. Marini. Unified analysis of discontinuous galerkin methods for elliptic problems. *SIAM J. Numer. Anal., Vol. 39(5), pp. 1749-1779*, 2002.

[14] M. Botti, D.A. di Pietro, and P. Sochala. A hybrid high-order method for nonlinear elasticity. *SIAM J. Numer. Anal., 2017, Vol. 55(6), pp. 2687-2717*, 2018.

[15] F. Brezzi, K. Lipnikov, and M. Shashkov. Convergence of the mimetic finite difference method for diffusion problems on polyhedral meshes. *SIAM J. Numer. Anal., Vol. 43(5), pp. 1872-1896*, 2005.

[16] F. Brezzi, K. Lipnikov, and V. Simoncini. A family of mimetic finite difference methods on polygonal and polyhedral meshes. *Math. Models Methods Appl. Sci., Vol. 15(10), pp. 1533-1551*, 2005.

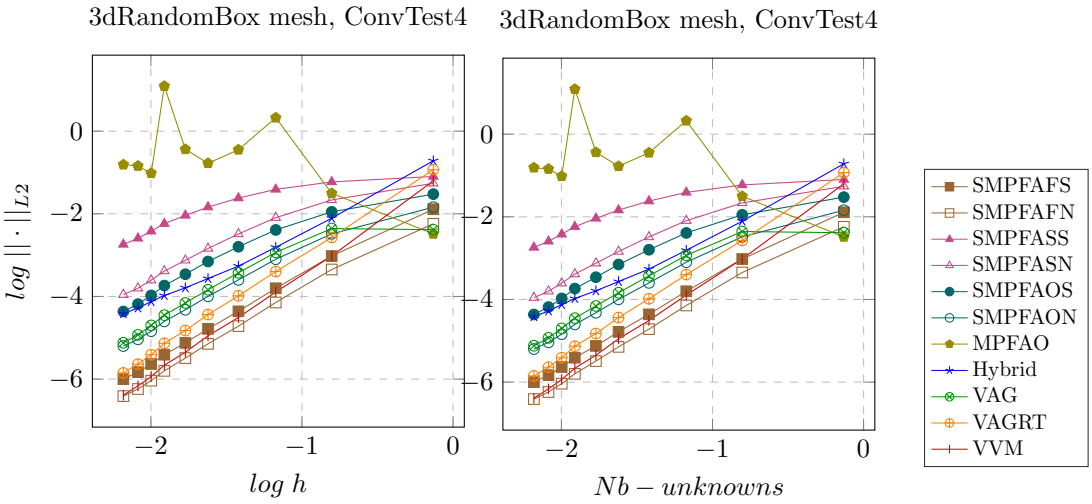

Figure 19: Convergence curves for *Sinusoidal3D* for the *3dRandomBox* mesh sequence

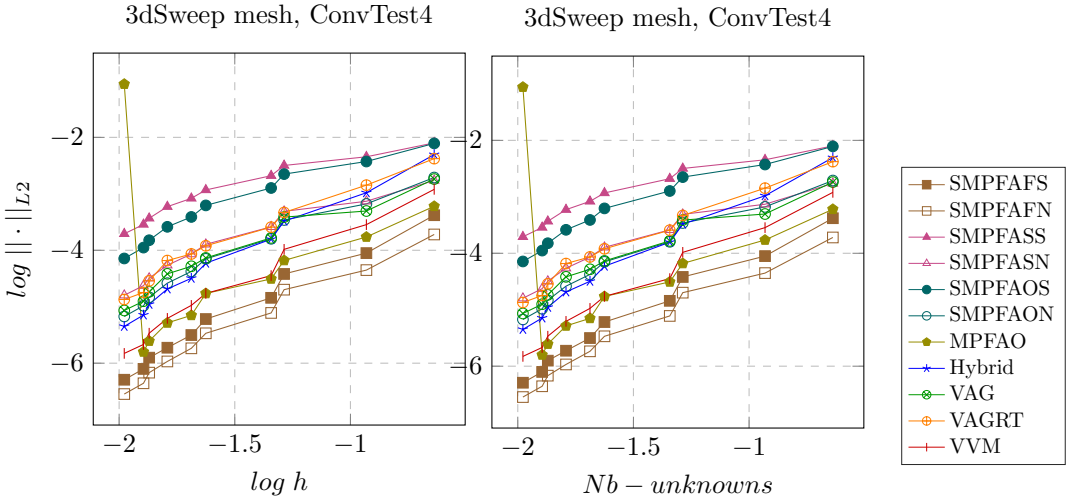

Figure 20: Convergence curves for *Sinusoidal3D* for the *3dSweep* mesh sequence

[17] F. Chave, D.A. di Pietro, and L. Formaggia. A hybrid high-order method for darcy flows in fractured porous media. *SIAM J. Sci. Comput., Vol. 40(2), pp. 1063-1094*, 2018.

[18] Q.-Y. Chen, J. Wan, Y. Yang, and R. T. Mifflin. Enriched multi-point flux approximation for general grids. *J. Comp. Phys. Vol. 227 pp. 1701-1721*, 2008.

[19] J. Coatléven. Semi hybrid method for heterogeneous and anisotropic diffusion problems on general meshes. *ESAIM Math. Model. Numer. Anal., Vol. 49, pp. 1063-1084*, 2015.

[20] J. Coatléven. A virtual volume method for heterogeneous and anisotropic diffusion-reaction problems on general meshes. *ESAIM Math. Model. Numer. Anal., Vol. 51, pp. 797-824*, 2017.

[21] B. Cockburn, J. Gopalakrishnan, and A. Lazaro. Unified hybridization of discontinuous galerkin, mixed and con-

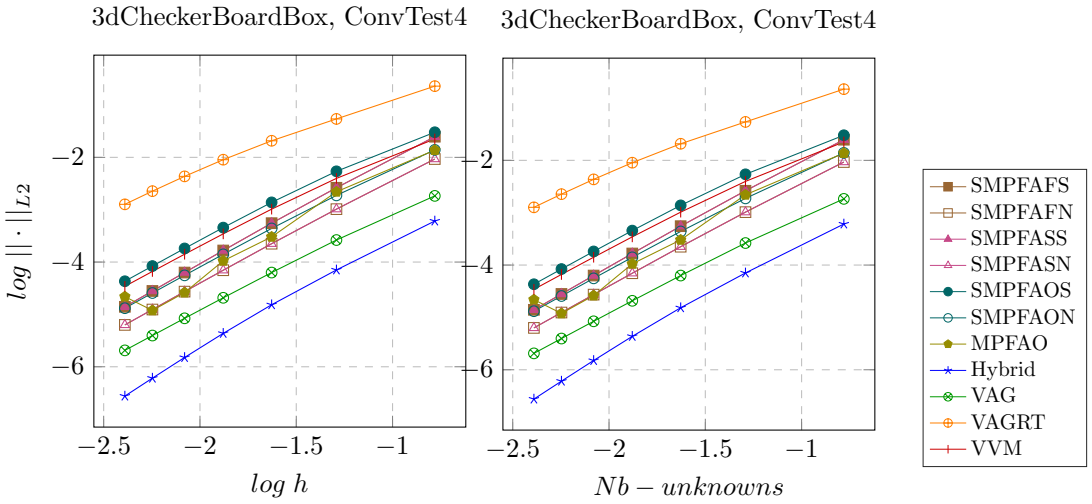

Figure 21: Convergence curves for *Sinusoidal3D* for the *3dCheckerBoardBox* mesh sequence

tinuous galerkin methods for second order elliptic problems. *SIAM J. Numer. Anal. Vol. 47(2), pp/ 1319-1365*, 2009.

[22] L. Beirao da Veiga. A mimetic discretization method for linear elasticity. *ESAIM Math. Model. Numer. Anal., vol. 44, pp. 231-250*, 2010.

[23] L. Beirao da Veiga, F. Brezzi, A. Cangiani, G. Manzini, L.D. Marini, and A. Russo. Basic principles of virtual element methods. *Math. Models Methods Appl. Sci., Vol. 23(1), pp. 199-214*, 2013.

[24] L. Beirao da Veiga, F. Brezzi, and L. D. Marini. Virtual elements for linear elasticity problems. *SIAM J. Numer. Anal., Vol. 51(2), pp.794-812*, 2013.

[25] L. Beirao da Veiga, K. Lipnikov, and G. Manzini. *The Mimetic Finite Difference Method for Elliptic Problems*. Springer, 2014.

[26] L. Beirao da Veiga, C. Lovadina, and D. Mora. A virtual element method for elastic and inelastic problems on polytope meshes. *Computer Methods in Applied Mechanics and Engineering, Vol. 295, pp. 327-346*, 2015.

[27] L. Beirao da Veiga, C. Lovadina, and G. Vacca. Divergence free virtual elements for the stokes problem on polygonal meshes. *ESAIM Math. Model. Numer. Anal., Vol. 51(2), pp. 509-535*, 2017.

[28] C. Dawson, S. Sun, and M. F. Wheeler. Compatible algorithms for coupled flow and transport. *Comp. Meth. Appl. Mech. Eng., vol. 193 pp. 2565-2580*, 2004.

[29] D. A. di Pietro and A. Ern. *Mathematical aspects of discontinuous Galerkin methods*. Springer, 2012.

[30] D.A. di Pietro and A. Ern. Discrete functional analysis tools for discontinuous galerkin methods with application to the incompressible navier-stokes equations. *Math. of Comp., Vol. 79 (271), pp. 1303–1330*, 2010.

[31] D.A. di Pietro and A. Ern. A hybrid high-order locking-free method for linear elasticity on general meshes. *Comput. Meth. Appl. Mech. Engrg., Vol. 283, pp. 1-21*, 2015.

[32] D.A. di Pietro and A. Ern. Hybrid high-order methods for variable-diffusion problems on general meshes. *C. R. Acad. Sci. Paris, Ser. I, Vol. 353, pp. 31-34*, 2015.

[33] J. Droniou. Finite volume schemes for diffusion equations : introduction to and review of modern methods. *Math. Models Methods Appl. Sci., Vol. 24(8), pp. 1575-1619, special edition "P.D.E. Discretizations on Polygonal Meshes"*, 2014.

[34] J. Droniou and R. Eymard. A mixed finite volume scheme for anisotropic diffusion problems on any grid. *Numer. Math. 105 (1), pp. 35-71*, 2006.

[35] J. Droniou, R. Eymard, T. Gallouët, and R. Herbin. A unified approach to mimetic finite differences, hybrid finite volume and mixed finite volume methods. *IMA J. Num. Anal. 31 (4), pp. 1357-1401*, 2011.

[36] J. Droniou, R. Eymard, T. Gallouët, C. Guichard, and R. Herbin. *The Gradient Discretisation Method*. Springer, 2018.

[37] J. Droniou and N. Nataraj. Improved l^2 estimate for gradient schemes and super-convergence of the tpfa finite volume scheme. *IMA J. Num. Anal., Vol. 38(3), pp. 1254-1293*, 2017.

[38] M. G. Edwards and C. F. Rogers. A flux continuous scheme for the full tensor pressure equation. *Proceedings of the fourth European Conference on the Mathematics of Oil Recovery, Norway*, 1994.

[39] R. Eymard, T. Gallouët, and R. Herbin. Finite volume methods. In *P.G. Ciarlet and J.-L. Lions editors, Techniques of scientific computing Part III*, Handbook of Numerical Analysis, pages 713–1020. North-Holland, Amsterdam, 2000.

[40] R. Eymard, T. Gallouët, and R. Herbin. A new finite volume scheme for anisotropic diffusion problems on general grids: convergence analysis. *C. R., Math., Acad. Sci. Paris, Vol. 344(6), pp. 403-406*, 2007.

[41] R. Eymard, T. Gallouët, and R. Herbin. Discretisation of heterogeneous and anisotropic diffusion problems on general nonconforming meshes sushi: a scheme using stabilisation and hybrid interfaces. *IMA J. Num. Anal., 30(4), pp 1009-1043*, 2010.

[42] R. Eymard, C. Guichard, and R. Herbin. Small-stencil 3d schemes for diffusive flows in porous media. *ESAIM Math. Model. Numer. Anal., Vol. 46(2), pp. 265-290*, 2011.

[43] R. Eymard, C. Guichard, R. Herbin, and R. Masson. Vertex-centred discretization of multiphase compositional darcy flows on general meshes. *Comput. Geosci., Vol. 16, pp. 987-1005*, 2012.

[44] R. Eymard, C. Guichard, R. Herbin, and R. Masson. Vertex centred discretization of two-phase darcy flows on general meshes. *ESAIM: Proc., Vol. 35, pp. 59-78*, 2012.

[45] J. M. Nordbotten and G. T. Eigestad. Discretization on quadrilateral grids with improved monotonicity properties. *J. Comp. Phys., Vol. 203(2), pp. 744-760*, 2005.

[46] D.A. Di Pietro. Cell centered galerkin methods for diffusive problems. *ESAIM Math. Model. Numer. Anal., Vol. 46(1), pp. 111-144*, 2012.

[47] R. Herbin R. Eymard, C. Guichard. Benchmark 3d : the vag scheme. *Springer proceedings in Mathematics, FVCA6, Prague, Vol. 2, pp. 213-222*, 2011.

[48] G. Vacca and L. Beirao da Veiga. Virtual element methods for parabolic problems on polygonal meshes. *Numerical Methods For Partial Differential Equations, Vol.31(6), pp. 2110-2134*, 2015.

[49] K. Wang, H. Wang, S. Sun, and M. F. Wheeler. An optimal-order l2-error estimate for nonsymmetric discontinuous galerkin methods for a parabolic equation in multiple space dimensions. *Comput. Methods Appl. Mech. Engrg. Vol. 198 pp. 2190-2197*, 2009.